Chaos, Solitons & Fractals 53 (2013) 18–33

Contents lists available at SciVerse ScienceDirect

Chaos, Solitons & Fractals

Nonlinear Science, and Nonequilibrium and Complex Phenomena

journal homepage: www.elsevier.com/locate/chaos

Renormalization group approach to chaotic strings

Stefan Groote [a,b,*], Hardi Veermäe [b], Christian Beck [c]

[a] Institut für Physik der Johannes-Gutenberg-Universität, Staudinger Weg 7, 55099 Mainz, Germany
[b] Füüsika Instituut, Tartu Ülikool, Tähe 4, 51010 Tartu, Estonia
[c] School of Mathematical Sciences, Queen Mary University of London, Mile End Road, London E1 4NS, UK

ARTICLE INFO

Article history:
Received 11 December 2012
Accepted 22 April 2013
Available online 25 May 2013

ABSTRACT

Coupled map lattices of weakly coupled Chebychev maps, so-called chaotic strings, may have a profound physical meaning in terms of dynamical models of vacuum fluctuations in stochastically quantized field theories. Here we present analytic results for the invariant density of chaotic strings, as well as for the coupling parameter dependence of given observables of the chaotic string such as the vacuum expectation value. A highly nontrivial and selfsimilar parameter dependence is found, produced by perturbative and nonperturbative effects, for which we develop a mathematical description in terms of suitable scaling functions. Our analytic results are in good agreement with numerical simulations of the chaotic dynamics.

1. Introduction

Coupled map lattices (CMLs), as introduced in seminal papers by Kaneko and Kapral some 29 years ago [1,2], are known to exhibit a rich structure of complex dynamical phenomena [3–7]. Of particular interest are CMLs that consist of locally chaotic maps. For hyperbolic local maps and very small coupling it can be proved [8–11] that a smooth invariant density of the entire CML exists and that there is ergodic behaviour. However, the case of nonhyperbolic local maps, e.g., of local 1-dimensional maps for which the slope is equal to zero at some point, is much more complicated from a mathematical point of view, and much less analytic results are known [12–18]. This is the realm of chaotic strings.

Chaotic strings are 1-dimensional coupled map lattices of diffusively coupled Chebychev maps [18]. They are intrinsically non-hyperbolic, since the local maps have an extremum with vanishing slope. They play a very important role in generalized statistical mechanics models of vacuum fluctuations [4,19–21], replacing the noise in stochastically quantized field theories by a deterministic chaotic dynamics [22–24]. These type of chaotic theories are of utmost interest in extensions of the standard model where one constructs additional sectors of rapidly fluctuating chaotic fields. One possible physical embedding is to associate the vacum energy generated by the chaotic strings with dark energy [25]. For more details on physical applications of chaotic strings in high energy physics, see Ref. [4].

In this paper, however, we will not deal with the above mentioned physical applications of chaotic strings, but merely concentrate onto the mathematics of these nonhyperbolic coupled map lattices. There is a highly interesting selfsimilar dependence of the invariant density on the coupling constant a of the CML, which can be understood by analytic means and which will be the main subject of this paper.

Let us first recall what has been done so far. In Refs. [19,20] weakly coupled N-th order Chebyshev maps [18,24–27] were studied and it was shown that certain scaling properties with respect to the coupling a can be calculated perturbatively. However, the fine structure of the parameter dependence of important observables of the chaotic string, such as the self energy or vacuum expectation value, could not be explained by these perturbative

* Corresponding author at: Institut für Physik der Johannes-Gutenberg-Universität, Staudinger Weg 7, 55099 Mainz, Germany.
E-mail address: groote@thep.physik.uni-mainz.de (S. Groote).

0960-0779/$ - see front matter © 2013 Elsevier Ltd. All rights reserved.
http://dx.doi.org/10.1016/j.chaos.2013.04.004

methods. In Ref. [28] is was numerically illustrated that the fine structure does occur only for CMLs of dimension 1, and not on lattices of higher dimension. In Ref. [29] short chaotic strings, consisting only of a small number of lattice points, were analyzed and it was shown that some of these short strings (with lengths between 3 and 5 lattice sites) show the same fine structure as long strings of the order of 10 000 sites, while for other short strings the fine structure had a totally different shape.

In this paper we report on significant progress to better understand the scaling structure of chaotic strings. We will show that the invariant density can not only be understood near the edges of the interval on which the local maps are defined, but in the entire interval region. We will study the coupling constant dependence of the expectation value of the chaotic field variable. This expectation is expressed as a particular integral, which is trivial for the uncoupled case (coupling $a = 0$) but exhibits a highly nontrivial parameter dependence for $a \neq 0$. There are certain invariance properties of observables of the chaotic string under suitable rescaling of the coupling that we will describe in terms of a kind of renormalization group theory. For this purpose we introduce two basic scaling functions, which we call 'draft function' and 'blunt function', which describe how parameter changes of the coupling are generating a self-similar pattern and how certain 'excitations' (travelling maxima) in the invariant density are induced. We also further develop the perturbation theory, and illustrate that there are perturbative and nonperturbative effects for the chaotic string, with certain analogy to what is known in quantum field theories.

This paper is organized as follows. In Section 2 we globalize the perturbative methods developed in Refs. [19,20] and apply them to the vacuum expectation value $\langle\phi\rangle$ of the chaotic field variable. In Section 3 we analyse the integrand leading to $\langle\phi\rangle$ and introduce draft and blunt functions which can help to analytically describe the self-similar parameter dependence and invariance properties of the chatic string. In Section 4 we discuss simplified models of the scaling structure which are connected to the perturbation theory. In Section 5 we look at limiting cases for the partition integrals that occur when the vacuum expectation is calculated. In Section 6 we provide analytical expressions for the (exponential-type) draft function. Finally, in Section 7 we draw our conclusions. More details on explicit calculations can be found in the Appendices.

2. The perturbative method

As shown in Ref. [20] in detail, the scaling behaviour of the self energy (and interaction energy) of the chaotic string based on Chebyshev maps $T_N(\phi)$ of order N is directly related to the scaling behaviour of the distribution function (the 1-point invariant density) $\rho(\phi)$ of the string. For the chaotic string of type 2B (cf. Ref. [4]) with iterative prescription

$$\begin{aligned}\phi_i^{n+1} &= (1-a)T_2(\phi_i^n) + \frac{a}{2}(\phi_{i+1}^n + \phi_{i-1}^n)\\ &=: T_{2a}(\phi_i^n; \phi_{i+1}^n + \phi_{i-1}^n)\end{aligned} \tag{1}$$

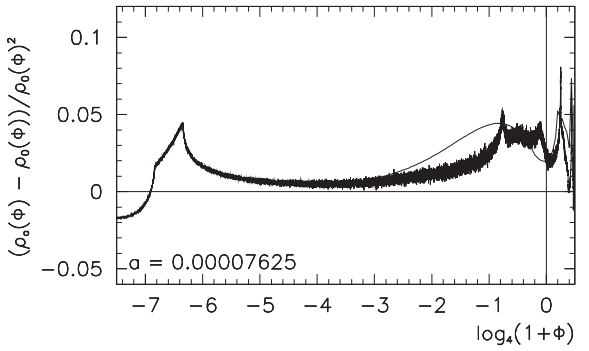

Fig. 1. Numerical result obtained by (a) long-term iteration of the CML and (b) the analytic approximation (5) at maximal order $p_{\max} = 7$. The figure shows the rescaled distribution function $(\rho_a(\phi) - \rho_0(\phi))/\rho_0^2(\phi)$ at coupling $a = 0.00007625$ close to the lower boundary $\phi = -1$ in dependence on $\log_4(1+\phi)$.

the distribution function close to the upper boundary $\phi = 1$ turned out to be a sum $\rho_a(1-ax) \approx \sum_{p=1}^{p_{\max}} \rho_a^{(p)}(1-ax)$ of functions $\rho_a^{(p)}$ (in the following sometimes called p-iterates) with[1]

$$\begin{aligned}\rho_a^{(p)}(1-ax) = &\frac{1}{\pi\sqrt{2a(1-a)}}\\ &\times \int \frac{\rho_0(\phi_+)d\phi_+\rho_0(\phi_-)d\phi_-}{4^p\sqrt{x/4^p - r_2^p(\phi_+) - r_2^p(\phi_-)}}\end{aligned} \tag{2}$$

while close to the lower boundary $\phi = -1$ we obtain $\rho_a(ay-1) \approx \rho_a^{(0)}(ay-1)$ with

$$\begin{aligned}\rho_a^{(0)}(ay-1) = &\frac{1}{\pi\sqrt{2a(1-a)}}\\ &\times \int \frac{\rho_0(\phi_+)d\phi_+\rho_0(\phi_-)d\phi_-}{\sqrt{y - (\phi_+ + \phi_-)/2 - 1}}.\end{aligned} \tag{3}$$

$\rho_0(\phi) = 1/\pi\sqrt{1-\phi^2}$ is the invariant density for the uncoupled string ($a = 0$). We use the notation $\phi_+ := \phi_{i+1}^n$, $\phi_- := \phi_{i-1}^n$, $\phi := \phi_i^n$, and

$$r_N^p(\phi) := \frac{1}{2}\sum_{q=0}^{p}\frac{1 - T_{N^q}(\phi)}{N^{2q}}. \tag{4}$$

Both approximations can be formally combined to the formula

$$\rho_a(\phi) = \sum_{p=0}^{p_{\max}} \rho_a^{(p)}(\phi) \tag{5}$$

This approximation is valid only close to the boundaries $\phi = \pm 1$. This is shown in Fig. 1 (close to the lower boundary) and Fig. 2 (close to the upper boundary). For the main part of the interval $\phi \in [-1,1]$, however, there are large deviations between numerical results obtained by iteration of the CML and the above formula, regardless of the order $p_{\max}$ of the approximation. Nevertheless, a main result of

[1] Compared to Ref. [20] we use a different definition (4) for the function $r_N^p(\phi)$ in order to keep it positive. Note that by convention the integration range is given by the positivity condition for the radicand [20].

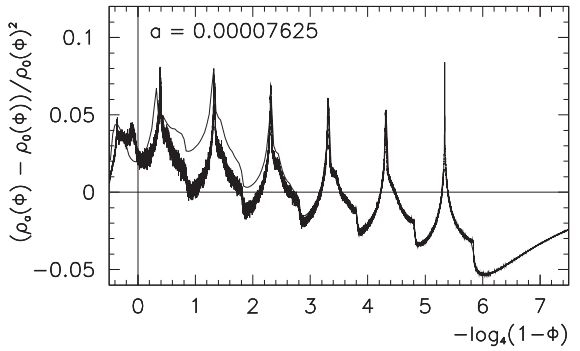

Fig. 2. Same as Fig. 1 but close to the upper boundary $\phi = +1$ in dependence on $-\log_4(1-\phi)$.

this paper is an extension to a formula that is valid for general values of ϕ.

2.1. Extension to the whole range

The key observation for this extension is given by the insight that the integrand of

$$\rho_a^{(0)}(\phi) = \frac{1}{\pi\sqrt{1-a}} \int \frac{\rho_0(\phi_+)d\phi_+\rho_0(\phi_-)d\phi_-}{\sqrt{2(\phi+1) - a(\phi_+ + \phi_- + 2)}} \tag{6}$$

is given by the derivative of the inverse map of the map (1),

$$\frac{1}{2\sqrt{1-a}\sqrt{2(\phi+1) - a(\phi_+ + \phi_- + 2)}} = \frac{d}{d\phi} T_{2a}^{-1}(\phi; \phi_+ + \phi_-) =: T_{2a}^{-1\prime}(\phi; \phi_+ + \phi_-). \tag{7}$$

Of course, the inverse $T_{2a}^{-1}(\phi; \phi_+ + \phi_-)$ of the function $T_{2a}(\phi; \phi_+ + \phi_-)$ given by the quadratic Eq. (1) with $T_2(\phi) = 2\phi^2 - 1$ is not unique. We have used the positive square root $T_{2a}^{+}(\phi; \phi_+ + \phi_-)$ according to the notation

$$T_{2a}^{\pm}(\phi; \phi_+ + \phi_-) := \pm\sqrt{\frac{2(\phi+1) - a(\phi_+ + \phi_- + 2)}{4(1-a)}} = T_{2a}^{-1}(\phi; \phi_+ + \phi_-) \tag{8}$$

in order to write

$$\rho_a^{(0)}(\phi) = \frac{2}{\pi} \int \rho_0(\phi_+)d\phi_+\rho_0(\phi_-)d\phi_- \frac{d}{d\phi} T_{2a}^{+}(\phi; \phi_+ + \phi_-). \tag{9}$$

Proceeding to the first iterate, we extend to

$$\rho_a^{(1)}(\phi) = -\frac{2}{\pi} \int \rho_0(\phi_+)d\phi_+\rho_0(\phi_-)d\phi_- \times \frac{d}{d\phi} T_{2a}^{+}\big(T_{2a}^{-}(\phi; T_2(\phi_+) + T_2(\phi_-)); \phi_+ + \phi_-\big). \tag{10}$$

For details of this and the following see Appendix A. For an arbitrary order p we finally arrive at

$$\rho_a^{(p)}(\phi) = -\frac{2}{\pi} \int \rho_0(\phi_+)d\phi_+\rho_0(\phi_-)d\phi_- \times \frac{d}{d\phi} T_{2a}^{+}\big(T_{2a}^{+}\big(\ldots T_{2a}^{-}\big(\phi; T_{2^p}(\phi_+) + T_{2^p}(\phi_-)\big)\ldots; T_2(\phi_+) + T_2(\phi_-)\big); \phi_+ + \phi_-\big). \tag{11}$$

2.2. The "path of roots"

The path "$+\cdots+-$" for selecting the nested square roots turns out to lead to an excellent approximation close to the upper limit $\phi = +1$. Of course we have to ask why this path needs to be taken and not a different one. The answer to this question is related to the trajectory that a starting value close to zero takes under nearly unperturbed iterations. Starting from $\phi = 0$ we obtain $T_2(0) = -1$, $T_2(T_2(0)) = +1$, $T_2(T_2(T_2(0))) = +1$ and so forth. This is just the time-reverse of the relevant "path of roots". However, if we want to extend the approximation of the invariant density in the way mentioned above, we need to take into account all paths. It turns out that a great amount of other paths returns contributions of lower order. Moreover, these contributions add up in a way that a general factor $2/\pi$ is factored out. The final result (understood as sum over all paths of roots)

$$\rho_a^{(p)}(\phi) = \int \rho_0(\phi_+)d\phi_+\rho_0(\phi_-)d\phi_- \times \frac{d}{d\phi} T_{2a}^{-1}\Big(T_{2a}^{-1}\Big(T_{2a}^{-1}\big(\ldots;(\phi;\ldots)\ldots;T_2(T_2(\phi_+)) + T_2(T_2(\phi_-))\big); T_2(\phi_+) + T_2(\phi_-)\Big); \phi_+ + \phi_-\Big) \tag{12}$$

for *a single* p-iterate (without adding lower iterates) approximates the distribution function to an increasing degree with increasing order p. More details on the derivation of the above equation can be found in Appendix B.

In Fig. 3 the coincidence of higher p-iterates with the distribution function is shown. For the coupling we have chosen a rather high value $a = 0.00122$ as we are no longer interested in the perturbative region close to the boundary but in nonperturbative effects in the middle of the interval. As compared to Figs. 1 and 2, the position and magnitude of the local maxima (often called 'excitations' in the following) are mirrored in a precise way. Even the excitation close to $\phi = -0.15$, i.e., in a highly nonperturbative region, is exactly modeled.

The excitation at $\phi \approx -0.15$ is special. Indeed, if we look at a sequence of diagrams similar to Fig. 3 where the coupling a gradually decreases, then this excitation moves to the left while all others move to the right. These and other counter movements account for the so-called 'fine

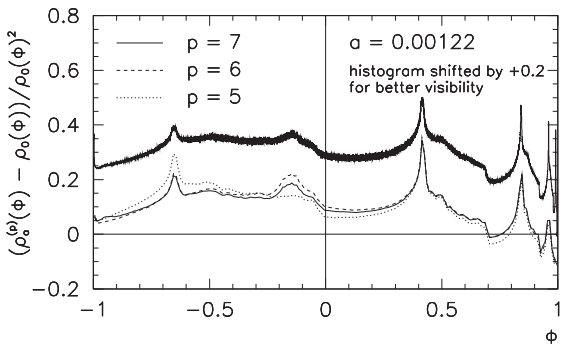

Fig. 3. Comparison of the rescaled $\rho_a^{(p)}(\phi)$ ($p = 5,6,7$) with the numerically obtained histogram result. In this plot the histogram is shifted by the amount +0.2 for better visibility.

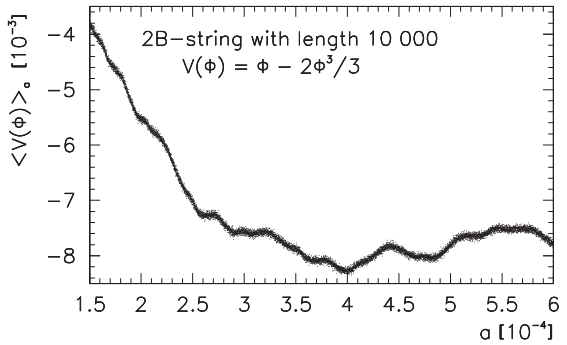

Fig. 4. Expectation value of the self energy $V(\phi)$ in the range $a \in [0.00015, 0.00060]$ for a 2B-string of 10,000 lattice points and 10,000 iterations.

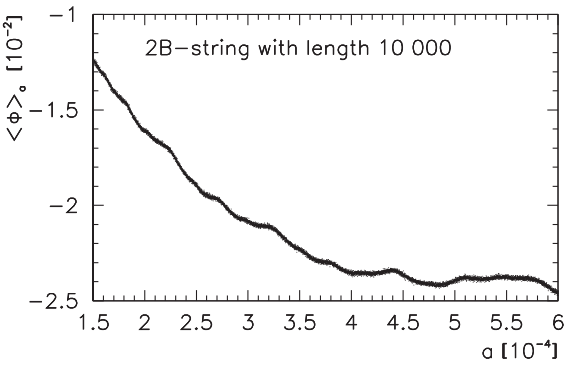

Fig. 5. Expectation value of ϕ in the range $a \in [0.00015, 0.00060]$ for a 2B-string of 10,000 lattice points and 10 000 iterations.

structure' of observables of the chaotic string. By this we mean a nontrivial local a-dependence of observables as illustrated, e.g., in Figs. 4 and 5. The reason for the different behaviour of the above excitation is that this excitation belongs to a different "path of roots" than the ordinary one ("$+\cdots+-$"). It can be associated with a process that is mirrored at the lower boundary. This becomes apparent when we look at a sequence of diagrams as in Fig. 3 again. At the moment when the extraordinary excitation disappears at $\phi = -1$, a new ordinary excitation appears at this point and moves to the right.

2.3. Expectations of observables

The fine structure we are trying to understand in this paper is the a-dependence of observables (functions of ϕ) such as, e.g., the self energy $V(\phi) = \phi - 2\phi^3/2$ calculated with respect to the distribution function $\rho_a(\phi)$ (cf. Fig. 4). These types of expectations of observables as a function of a turn out to be of utmost interest for the physical applications described in Ref. [4]. It turns out that the vacuum expectation value $\langle\phi\rangle$ of the string leads to the same (but less pronounced) fine structure, as it is shown in Fig. 5. Therefore, in the following we will concentrate onto the calculation of $\langle\phi\rangle = \int \phi\rho_a(\phi)$. Approximating $\rho_a\ (\phi)$ by the p-iterate $\rho_a^{(p)}(\phi)$, one can perform a $(p+1)$-fold integration by parts to obtain

$$\begin{aligned}\langle\phi\rangle_a &= \int \phi\rho_a^{(p)}(\phi)d\phi \\ &= \int \rho_0(\phi_+)d\phi_+\rho_0(\phi_-)d\phi_- \\ &\quad\times T_{2a}(T_{2a}(T_{2a}(\ldots T_{2a}(\phi^{(p)};\phi_+ + \phi_-)\ldots; \\ &\qquad T_{2^{p-2}}(\phi_+) + T_{2^{p-2}}(\phi_-)); T_{2^{p-1}}(\phi_+) + T_{2^{p-1}}(\phi_-)); \\ &\qquad T_{2^p}(\phi_+) + T_{2^p}(\phi_-))d\phi^{(p)}. \end{aligned} \tag{13}$$

This equation reminds us of results obtained in Ref. [29] for an open string of length 3.[2] In order to better understand how the excitation can switch to a different "path of roots"

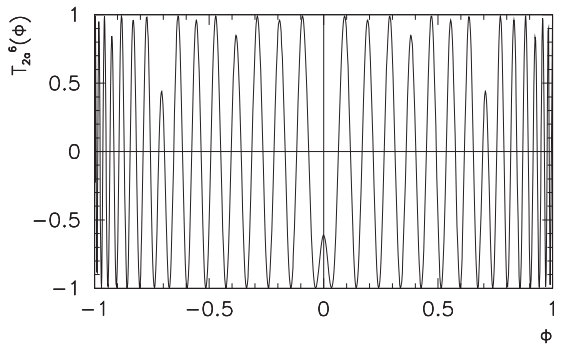

Fig. 6. Integrand of Eq. (13) for $p = 5$ at $a = 0.00122$ and $\phi_- = \phi_+ = 1$.

if a is changed we take a detailed look at the integrand in Eq. (13) as a function of $\phi^{(p)}$ (renamed as ϕ) for different values of (ϕ_+, ϕ_-). For $(\phi_+, \phi_-) = (+1, +1)$ the integrand at $a = 0.00122$ is shown in Fig. 6. We see that while the minima of this strongly oscillating function take the value -1, some of the maxima take values less than *1*. The most extreme situation is found at $\phi = 0$ where the maximum is on the way to decay completely if a changes in a significant way. When this happens, the two neighbouring minima unite into one new minimum. From the calculations in Refs. [19,20] it can be seen that the height of maxima is related to excitations of the distribution function. The decay of a maximum at $\phi = 0$ for increasing values of a thus means that an excitation ceases to exist at the lower boundary. The vanishing of the extraordinary excitation mentioned before is related to such a formation of a united minimum.

3. Structural changes of the generating partition

The change described before is a change of the topological structure because one of the local oscillations which partitions the interval $[-1,1]$ into 2^p intervals vanishes. Indeed, the different partitions stand in direct correspondence to the different roots of the integrand. For vanishing coupling $a = 0$ the maxima and minima are located exactly at $\sin(\pi t/2)$ for the values $t = \pm 2n/2^p$ and $t = \pm(2n+1)/2^p$, respectively, where $n = 0,1,\ldots,2^{p-1}$ counts the extrema. The minima divide the interval $[-1,1]$ into

[2] Note that due to a numerical error, in Ref. [29] is was erroneously stated that the open string of length 3 does not reproduce the fine structure. This will be corrected in an erratum to Ref. [29].

2^p intervals which we call the elements of the generating partition (see Fig. 6). If one of these elements vanishes, the topological structure of the partition changes.

One can use the generating partition to split up the integral in Eq. (13) into a sum of 2^p partition integrals. From this point of view, the decay of a maximum means the vanishing of the corresponding partition integral. In the following we take a closer look on how an increasing coupling a influences the contribution of the integrand through the different elements of the generating partition. In order to distribute the elements of the generating partition uniformly onto the interval $[-1,1]$, we use a new variable t, with $\phi = \sin(\pi t/2)$.

3.1. Decay of the maxima

A general feature of the integrand is that maxima which for $a = 0$ are located at equally spaced positions ("starting positions") t_0 decay in a similar way when a is increased. This property forms the basis for our renormalization group approach in the following. Let us assign a class k to certain subsets of maxima as follows: The maxima with starting positions $t_0 = 0$ and ± 1 are of class $k = 0$, the maxima with starting positions $t_0 = \pm 1/2$ are of class $k = 1$, the maxima with starting positions $t_0 = \pm 1/4, \pm 3/4$ are of class $k = 2$, and so on. In general, the starting positions of class k are given by $t_0 = \pm(2n+1)/2^k$, $n = 0,1,\ldots,2^{k-1}-1$. We note the similarity with the definition of k-cylinders in the thermodynamic formalism of dynamical systems [34]. For $(\phi_+,\phi_-) = (+1,+1)$ the height of a maximum of class k is given by

$$b = \cos\left(\sqrt{a}2^{p-k+1}\right). \tag{14}$$

From Eq. (14) we read off that for a specified scaling interval where a increases by a factor 4 (e.g., $a \in [0.00015, 0.00060]$), precisely one single specified class of maxima (and, therefore, partition integrals) disappears, and this disappearence takes place synchronously. Apparently the successive decay of maxima produces global scaling features, such as the invariance under the transformation $a \to 4a$, but it is not responsible for the fine structure within a given scaling region, which is more related to infinitesimal changes of a. To better understand the fine structure, in the following we will introduce two important auxiliary functions: Draft functions and blunt functions.

3.2. The draft function

If elements of the generating partition vanish, the neighbouring partition elements fill the gap, being drawn close to the position where the topological change happens. The difference between the starting position of a given maximum and the position for $a \neq 0$ turns out to be a linear function in a. The slope, therefore, is a well-defined function called draft function, $d(\phi_0) = d\phi_a(a;\phi_0)/da$ where $\phi_a(a;\phi_0)$ is the position of the maximum with $\phi_a(0;\phi_0) = \phi_0$. For large p and k this is a fractal function, and the basic features visible in a plot are independent of p and k. The function is shown in Figs. 7–9 for $(\phi_+,\phi_-) = (+1,+1)$, $(+1,-1)$ (which is the same as for $(-1,+1)$) and $(-1,-1)$. We found an analytical expression for the draft function. With $\phi_0 = \sin(\pi t_0/2)$ the analytical formula for the draft function of class k reads

$$\tilde{d}^{(k)}(t_0;\phi_+,\phi_-) = \frac{1}{2}\left(\tilde{d}^{(k)}(t_0;\phi_+) + \tilde{d}^{(k)}(t_0;\phi_-)\right) \tag{15}$$

(the tilde indicates the linearization of the first argument by replacing $\phi_0 = \sin(\pi t_0/2)$ by t_0) where

$$\tilde{d}^{(k)}(t_0;\phi_\pm) = \tilde{d}^{(k)}(t_0) + \sum_{l=0}^{k-1} T_{2^l}(-\phi_\pm)\tilde{d}_l^{(k)}(t_0) \tag{16}$$

and

$$\tilde{d}^{(k)}(t_0) = 2^{-k}d_{-1}^{(k)}(t_0) - \sum_{l=0}^{k-1}\left(2^{1-k+l} + \cos(2^l\pi t_0)\right)\tilde{d}_l^{(k)}(t_0),$$
$$\tilde{d}_l^{(k)}(t_0) = \frac{1}{2^l\pi\sin(2^l\pi t_0)}. \tag{17}$$

The draft function $\tilde{d}^{(k)}(t_0;\phi_+,\phi_-)$ is smooth for $t_0 = \pm(2n+1)/2^k$, $n = 0,1,\ldots,2^{k-1}-1$ but singular for values t_0 corresponding to a class smaller than k.

3.3. The blunt function

Eq. (14) is valid only for the specific value $(\phi_+,\phi_-) = (+1,+1)$ of the neighbours. For general neighbouring values ϕ_+, ϕ_- the height of maxima of class k is given by

$$b_{p,k}(\phi_+,\phi_-) = \cos\left(2^{p-k+1}\sqrt{a r_2^\infty(-T_{2^k}(\phi_+),-T_{2^k}(\phi_-))}\right) \tag{18}$$

where r_N^p is defined in Eq. (4). We call $b_{p,k}$ the 'blunt function'. Both draft and blunt functions are important for our renormalization group description in the following. Basically the draft function describes how positions of maxima change under parameter changes, and the blunt function describes how the values of the maxima themselves change.

If the integrand for different values of (ϕ_+,ϕ_-) is affected by a relative draft, the blunting is accelerated because after integration over $\rho_0(\phi_+)\rho_0(\phi_-)$ the integrand (in ϕ) is smeared out, giving rise to a premature breakdown of the integral.

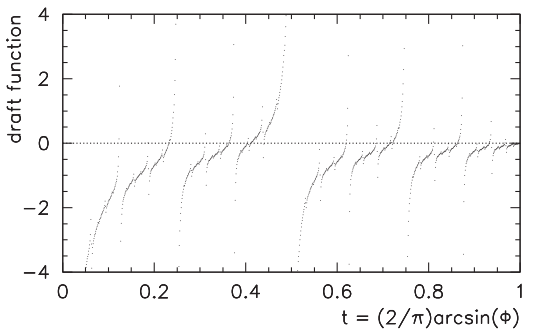

Fig. 7. Draft function for $\phi_+ = \phi_- = +1$.

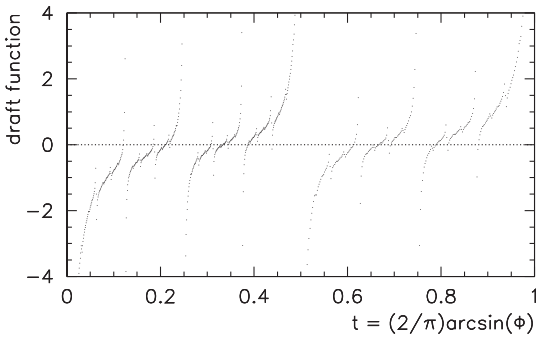

Fig. 8. Draft function for $\phi_+ = +1$ and $\phi_- = -1$.

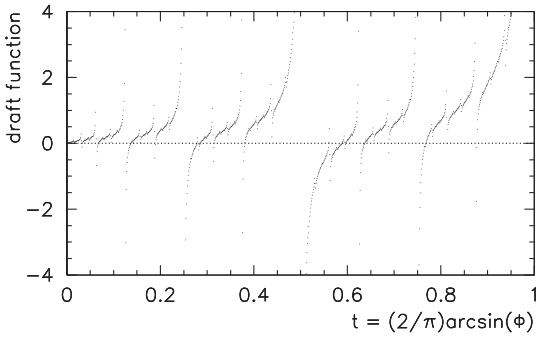

Fig. 9. Draft function for $\phi_+ = \phi_- = -1$.

4. Renormalisation group approach

The simultaneous parameter-dependent deformations described by draft and blunt functions are the basis for our treatment in the following. To understand the complex a-dependence of observables such as the vacuum expectation value, we need to evaluate the integral (13). This integral, as mentioned before, is split into many partition integrals. These partition integrals are defined as the part of the integral (13) where the integration range is restricted to the interval given by the positions t_a and t_b of two adjacent minima surrounding a decaying maximum with starting position t_0,

$$\langle\phi\rangle_a(t_0) = \frac{\pi}{2}\int_{t_a}^{t_b} f(t)\cos\left(\frac{\pi t}{2}\right)dt \tag{19}$$

where the integrand is given by

$$f(t) := \int \rho_0(\phi_+)\mathrm{d}\phi_+\rho_0(\phi_-)\mathrm{d}\phi_- \times T_{2a}(\ldots T_{2a}(\sin(\pi t/2);\phi_+ + \phi_-)\ldots;T_{2^p}(\phi_+) + T_{2^p}(\phi_-)). \tag{20}$$

In Figs. 10 and 11, we show a sequence of partition integrals and their sum for values of p and k with constant difference $p - k = 6$. At first sight one might conjecture that all these partition integrals vanish at the same maximal value of a, called the *maximal reach* for a given (p,k). However, our careful analysis shows that due to different values of the draft function, many partition integrals vanish at values below the maximal value for a given (p,k).

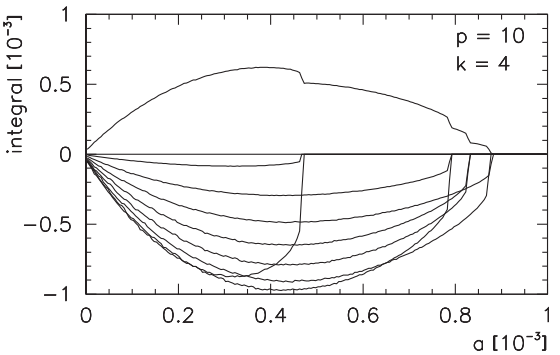

Fig. 10. Contributions and sum of all the partition integrals for $p = 10$ and $k = 4$ that vanish in the displayed interval for a. For better visibility, the sum is multiplied by -2^{1-k}.

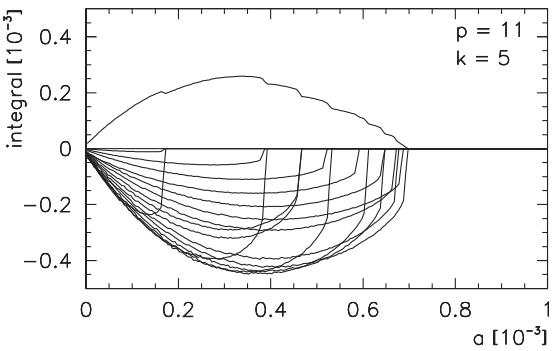

Fig. 11. Contributions and sum of all the partition integrals for $p = 11$ and $k = 5$ that vanish in the displayed interval for a. For better visibility, the sum is multiplied by -2^{1-k}.

Even though the draft function does not depend on p and k, the effect of partition integrals to vanish below the maximal reach increases with the order because the maxima are closer together and are smeared out faster. For this reason, also the maximal reach of the partition integrals (i.e., the value a at which all partition integrals of the same class vanish) is decreasing in the sequence of the two diagrams shown in Figs. 10 and 11.

In the spirit of a suitable renormalization group theory, we are now looking for a transition $p \to \infty$ that preserves the shape and sum of the partition integrals. Comparing the case $p = 14$, $k = 6$ as displayed in Fig. 12 with Fig. 10 ($p = 10$, $k = 4$), and the case $p = 13$, $k = 6$ in Fig. 13 with Fig. 11 ($p = 11$, $k = 5$), we find that the quantity to be kept constant is given by the *reduced order* $\dot{p} = p - 2k$ which in the two examples is given by $\dot{p} = 2$ and $\dot{p} = 1$, respectively. However, in Figs. 12 and 13 we have stretched the axis for a by a factor of 4 and 16, respectively. Because we are looking at the behaviour in the scaling region only, this means that instead of the coupling a one should use the *reduced coupling* $\hat{a} = 4^{p-k}a$ which for the intervals shown in Figs. 10–12 is found in the interval $\hat{a} \in [0,4]$. With the above rescaling prescriptions, the overall problem is formulated in a *scale invariant* way in the limit $p \to \infty$.

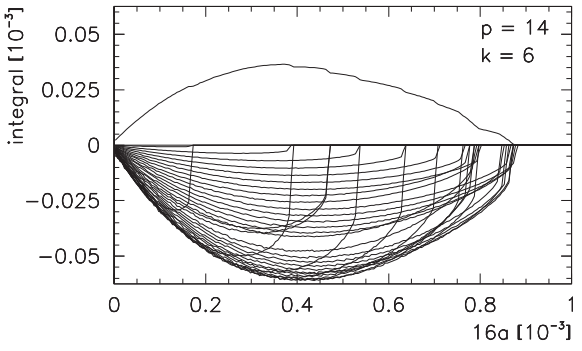

Fig. 12. Contributions and sum of all the partition integrals for $p = 14$ and $k = 6$ that vanish in the displayed interval. For better visibility, the sum is multiplied by -2^{1-k}.

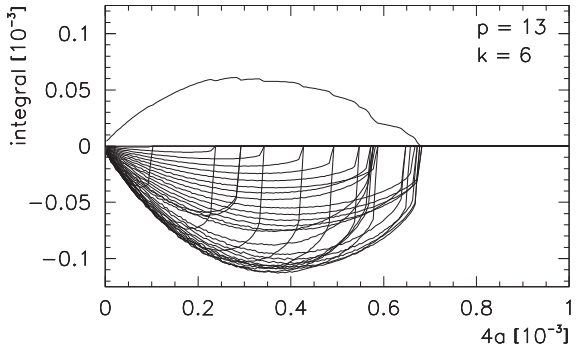

Fig. 13. Same as Fig. 12 but for $p = 13$ and $k = 6$.

4.1. The model function

The Feigenbaum fixed point function in Feigenbaum's renormalization group approach for 1-dimensional critical systems can be well approximated close to the vicinity of the maximum of the map [32–34]. Similarly, we can also find a good approximation of the integrand in our problem if we are close to a decaying maximum. We call this approximating function of the integrand the 'model function'. Using the analytical expressions for draft and blunt functions, the integrand in Eq. (20) in the region close to a decaying maximum is approximated by the model function

$$f(\Delta t;t_0)=\int_{-1}^{1}\rho_0(\phi_+)d\phi_+\rho_0(\phi_-)d\phi_-\times\cos\left(2^p\sqrt{\pi^2\left(\Delta t-a\tilde{d}^{(k)}(t_0;\phi_+,\phi_-)\right)^2+4^{1-k}ar_2^{\infty}(-T_{2^k}(\phi_+),-T_{2^k}(\phi_-))}\right) \tag{21}$$

which is derived from Eq. (18). This turns out to be a quite precise approximation for $f(t_0+\Delta t)$ in Eq. (20) where Δt is the deviation from the starting position t_0 of the specified maximum. If in addition to the reduced order and coupling one uses the *reduced deviation* $\Delta\hat{t}=2^p\Delta t\in[-1,1]$, the limit $p\to\infty$ can be performed for the model function (21), rewritten as

$$\begin{aligned}\hat{f}^{(\hat{p})}(\Delta\hat{t};t_0)&:=f(2^{-p}\Delta\hat{t};t_0)\\&=\int\rho_0(\phi_+)d\rho_+\rho_0(\phi_-)d\phi_-\\&\quad\times\cos\left(\sqrt{\pi^2\left(\Delta\hat{t}-2^{\hat{p}}\hat{a}\tilde{d}^{(k)}(t_0;\phi_+,\phi_-)\right)^2+2\hat{a}r_2^{\infty}(-T_{2^k}(\phi_+),-T_{2^k}(\phi_-))}\right).\end{aligned} \tag{22}$$

The function $r_2^{\infty}(\phi_+,\phi_-)$ uses the k-fold Chebyshev map for the arguments $\phi_\pm$ while the arguments of the draft function are just $\phi_\pm$. Keeping the reduced order $\hat{p}=p-2k$ constant, the class k increases together with the order p. Because of this, the high-frequency blunt can be separated from the low-frequency draft, leading to an effective blunt of 8/3 (see Appendix C). The final result for the model function in the limit $p\to\infty$ reads

$$\begin{aligned}\hat{f}^{(\hat{p})}(\Delta\hat{t};t_0)&=\int\rho_0(\phi_+)d\phi_+\rho_0(\phi_-)d\phi_-\\&\quad\times\cos\left(\sqrt{\pi^2\left(\Delta\hat{t}-2^{-\hat{p}}\hat{a}\tilde{d}^{(k)}(t_0;\phi_+,\phi_-)\right)^2+\frac{8\hat{a}}{3}}\right).\end{aligned} \tag{23}$$

4.2. Fourier transformation

We note that the integrand in the above Eq. (23) is essentially of the form $g(a,t):=\cos(\sqrt{t^2+a})$. Inspired by quantum field theory, we proceed to a Fourier transform denoted as

$$\tilde{g}(a,\omega)=\int_{-\infty}^{\infty}\cos(\sqrt{t^2+a})\cos(\omega t)dt. \tag{24}$$

It can be shown that $g(a,\omega)=0$ for $\omega^2>1$, but otherwise

$$\begin{aligned}\tilde{g}(a,\omega)&=2\pi\delta(1-\omega^2)\\&\quad-\frac{\pi a}{\sqrt{a(1-\omega^2)}}J_1\left(\sqrt{a(1-\omega^2)}\right),\end{aligned} \tag{25}$$

where $J_1(z)$ is the Bessel function of the first kind. One obtains

$$g(a,t)=\cos t-\int_{-1}^{+1}\frac{a\,d\omega}{2\sqrt{a(1-\omega^2)}}J_1\left(\sqrt{a(1-\omega^2)}\right)\cos(\omega t). \tag{26}$$

If this is inserted into Eq. (23), the model function can be expressed as

$$\begin{aligned}f^{(\hat{p})}(\Delta\hat{t};t_0)&=\int\rho_0(\phi_+)d\phi_+\rho_0(\phi_-)d\phi_-\\&\quad\times\Big[\cos(i\pi(\Delta\hat{t}-2^{-\hat{p}}\hat{a}\tilde{d}^{(k)}(t_0;\phi_+,\phi_-)))\\&\quad-\int_{-1}^{+1}\frac{4\hat{a}\;d\omega}{3\sqrt{8\hat{a}(1-\omega^2)/3}}J_1\left(\sqrt{8\hat{a}(1-\omega^2)/3}\right)\\&\quad\times\cos(i\pi\omega(\Delta\hat{t}-2^{-\hat{p}}\hat{a}\tilde{d}^{(k)}(t_0;\phi_+,\phi_-)))\Big].\end{aligned} \tag{27}$$

5. Limiting cases

Clearly the exact renormalization group treatment requires the limit $p \to \infty$. On the other hand, of relevance for a scale invariant formulation is the reduced order $\hat{p} = p - 2k$. In the following we look at different limiting behavior depending on the relative size of p and k. It turns out that one can distinguish two different limit ranges which we call the perturbative and the nonperturbative range.

5.1. The perturbative range

Increasing the reduced order $\hat{p}$, the maximal reach does not increase in the same way. Instead, more and more partition integrals vanish close to the maximal reach (see Fig. 14). This means that compared to the blunt effect, the draft effect can be neglected. Note the similarity of the three displayed pictures in Fig. 14, which is due to the fact that the reduced coupling $\hat{a} = 4^{p-k}a$ is used. This range of parameters p and k does not contribute to the fine structure but is responsible for the global selfsimilar behaviour of expectations of observables.

5.2. The nonperturbative range

More interesting for the fine structure is the case where the reduced order $\hat{p}$ becomes negative. Fig. 15 unveils a rich structure. While Fig. 15 is calculated by using the model function (27), the calculation for the open string of length 3 leads to the same result. Finally, the result for class $k = 9$ (with the same reduced order $\hat{p} = -3$, or $p = 15$) is again very similar. This means that the model function correctly describes the effects seen in this nonperturbative range. Very characteristic is the kink close to $\hat{a} = 0.5$ which is relevant for the fine structure. This kink has its origin in a majority of partition integrals swinging twice before they vanish.

5.3. Development of bounded states

Characteristic for the nonperturbative range is that for a given decaying maximum, the neighbouring maxima are influenced strongly by the decay of the central maximum. They decay nearly as fast as the central maximum. If we use as an analogy the language of particle physics, then maxima seem to interact and to formate something like a bounded state. An interesting open question is whether these "bounded states" can be described properly within our current formalism based on partitions, or whether a different approach is necessary for this.

6. The exponential draft function

In the following we will perform further calculations on the draft function, which will ultimately lead to the implementation of graph theoretical methods previously introduced in Refs. [30,31].

Our motivation is as follows. Higher-order correlations of uncoupled Chebychev maps have been previously calculated using a graph-theoretical method. The graphs relevant for N-th order Chebychev maps consist of forests of N-ary trees [30,31]. It is now intriguing that the same type of graphs can be used for the coupled map system when calculating the relevant scaling functions. This reminds us of the use of Feynman graphs in quantum field theory, where one also uses graphs up to a certain order to understand the coupled system.

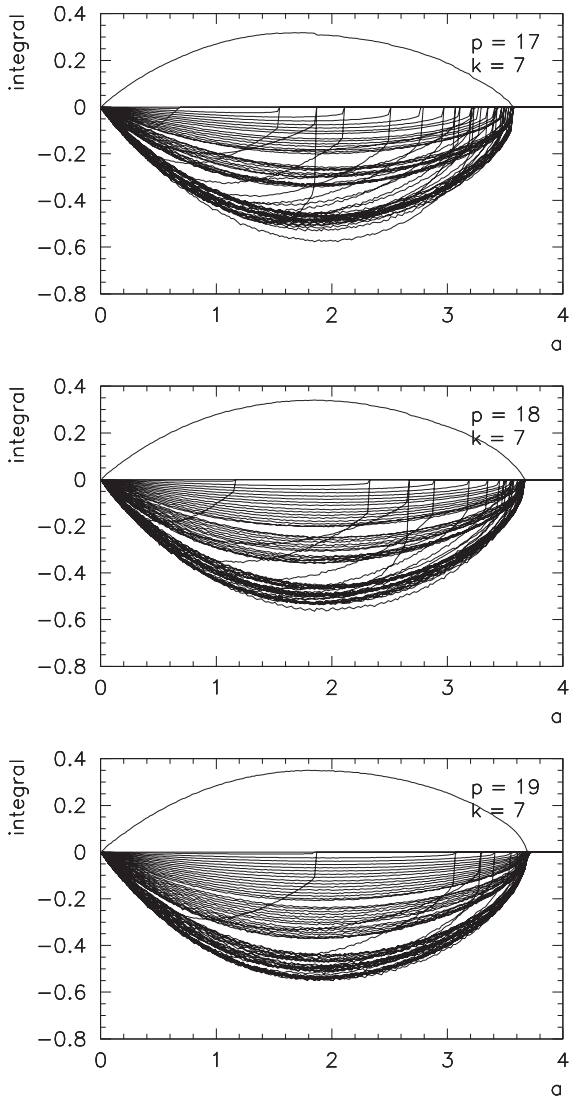

Fig. 14. Contributions and sum of partition integrals of class $k = 7$ for increasing order $p = 17, 18, 19$ (from top to bottom, corresponding to the reduced order $\hat{p} = 3, 4, 5$) as functions of $\hat{a}$. For better visibility, the sum is multiplied by -2^{1-k}.

Let us define an *exponential draft function* by

$$\tilde{h}(\omega; t_0) := \int_{-1}^{+1} \exp(-i\omega \tilde{d}^{(k)}(t_0; \phi_+))\rho_0(\phi_+)d\phi_+. \qquad (28)$$

With the help of this the model function can be written as

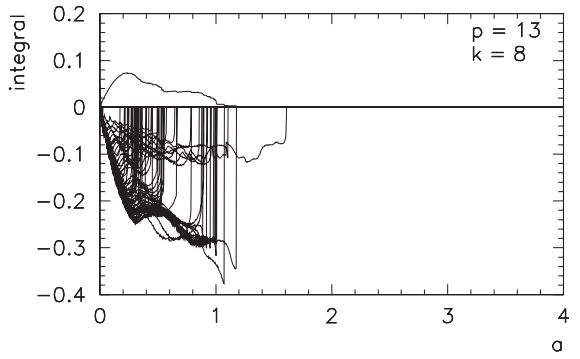

Fig. 15. Contributions and sum of partition integrals for $p = 13$ and $k = 8$ as a function of $\hat{a} \in [0,4]$. For better visibility, the sum is multiplied by -2^{1-k}.

$$f^{(\hat{p})}(\Delta t; t_0) = \mathrm{Re}(e^{i\pi\Delta t}\tilde{h}^2(2^{-\hat{p}-1}\pi\hat{a}; t_0)) - \int_{-1}^{+1} \frac{4\hat{a}\, d\omega}{3\sqrt{8\hat{a}(1-\omega^2)/3}} J_1\left(\sqrt{8\hat{a}(1-\omega^2)/3}\right) \times \mathrm{Re}\left(e^{i\pi\omega\Delta t}\tilde{h}^2(2^{-\hat{p}-1}\pi\hat{a}\omega; t_0)\right). \quad (29)$$

The relative minima (and maxima) of the model function which define the boundaries of the partition integrals are found by calculating the first derivative with respect to $\Delta\hat{t}$ and determining the zeros of this derivative. One obtains

$$\mathrm{Im}(e^{i\pi\Delta\hat{t}}\tilde{h}^2(2^{-\hat{p}-1}\pi\hat{a}; t_0)) = \int_0^1 \frac{8\hat{a}\omega\, d\omega}{3\sqrt{8\hat{a}(1-\omega^2)/3}} J_1\left(\sqrt{8\hat{a}(1-\omega^2)/3}\right) \times \mathrm{Im}\left(e^{i\pi\omega\Delta\hat{t}}\tilde{h}^2(2^{-\hat{p}-1}\pi\hat{a}\omega; t_0)\right), \quad (30)$$

using the fact that the integrand is an even function of ω.

The exponential draft function can be visualised by a parametric curve in the complex plane, as it is shown for $k = 8$, $p = 13$ and a particular partition integral specified by $n = 42$ in Fig. 16. The long range of the curve is due to the fact that $2^{-\hat{p}-1}\pi\hat{a} = 4\pi\hat{a}$ is not a small number. Note that the curve for $\omega \in [-1,0]$ is obtained by mirroring at the real axis. The parametric curve shows quite an irregular behaviour which is hard to predict.

6.1. Analytical expression for the exponential draft function

One can perform a concrete calculation to obtain the exponential draft function using graph theory. Inserting Eq. (16) into Eq. (28), one obtains[3]

$$\tilde{h}(\omega; t_0) = e^{-i\omega\tilde{d}^{(k)}(t_0)} \times \int_{-1}^{1} \exp\left(-i\omega\sum_{l=0}^{k-1} T_{2^l}(\phi_+)\tilde{d}_l^{(k)}(t_0)\right)\rho(\phi_+)d\phi_+ = e^{-i\omega\tilde{d}^{(k)}(t_0)}\sum_{n=0}^{\infty}\frac{(-i\omega)^n}{n!} \times \int_{-1}^{1}\left(\sum_{l=0}^{k-1} T_{2^l}(\phi_+)\tilde{d}_l^{(k)}(t_0)\right)^n \rho_0(\phi_+)d\phi_+. \quad (31)$$

[3] Without loss of generality, $T_{2^l}(-\phi_\pm)$ can be replaced by $T_{2^l}(\phi_\pm)$ under the integration.

In the following we use the short hand notations $d := \tilde{d}^{(k)}(t_0)$ and $d_l := \tilde{d}_l^{(k)}(t_0)$ and the convention that sums run over values where all indices under the sum take non-negative values less than k. By performing the integration over ϕ_+ one obtains

$$\begin{aligned}\tilde{h}(\omega; t_0) = e^{-i\omega d}\Bigg(&1 + \frac{(-i\omega)^2}{4}\sum d_l^2 + \frac{(-i\omega)^3}{8}\sum d_l^2 d_{l+1} \\ &+ \frac{(-i\omega)^4}{16}\sum d_l^2 d_{l+1}d_{l+2} + \frac{(-i\omega)^4}{32}\left(\sum d_l^2\right)^2 \\ &- \frac{(-i\omega)^4}{64}\sum d_l^4 + \frac{(-i\omega)^5}{32}\sum d_l^2 d_{l+1}d_{l+2}d_{l+3} \\ &+ \frac{(-i\omega)^5}{32}\sum d_l^2 d_{l+1}\sum d_{l'}^2 + \frac{(-i\omega)^5}{384}\sum d_l^4 d_{l+2} \\ &- \frac{(-i\omega)^5}{64}\sum d_l^2 d_{l+1}^3 - \frac{(-i\omega)^5}{48}\sum d_l^4 d_{l+1} \\ &+ \frac{(-i\omega)^6}{64}\sum d_l^2 d_{l+1}d_{l+2}d_{l+3}d_{l+4} \\ &+ \frac{(-i\omega)^6}{384}\sum d_l^2 d_{l+1}^3 d_{l+3} + \frac{(-i\omega)^6}{768}\sum d_l^4 d_{l+2}d_{l+3} \\ &- \frac{(-i\omega)^6}{48}\sum d_l^2 d_{l+1}^3 d_{l+2} - \frac{(-i\omega)^6}{96}\sum d_l^4 d_{l+1}d_{l+2} \\ &- \frac{(-i\omega)^6}{128}\sum d_l^2 d_{l+1}d_{l+2}^3 - 11\frac{(-i\omega)^6}{1536}\sum d_l^4 d_{l+1}^2 \\ &+ \frac{(-i\omega)^6}{64}\sum d_l^2 d_{l+1}d_{l+2}\sum_{l'=0}^{k-1} d_{l'}^2 \\ &+ \frac{(-i\omega)^6}{128}\left(\sum d_l^2 d_{l+1}\right)^2 + \frac{(-i\omega)^6}{576}\sum d_l^6 \\ &- \frac{(-i\omega)^6}{256}\sum d_l^4\sum d_{l'}^2 + \frac{(-i\omega)^6}{384}\left(\sum d_l^2\right)^3 + \cdots\Bigg). \end{aligned} \quad (32)$$

Expressing the higher-order correlation of (uncoupled) Chebyshev maps in terms of a graph theoretical approach [30,31], the various contributions above represent possible integer partitions of powers of *2* and can be represented as binary forests. It can be shown that the series can be

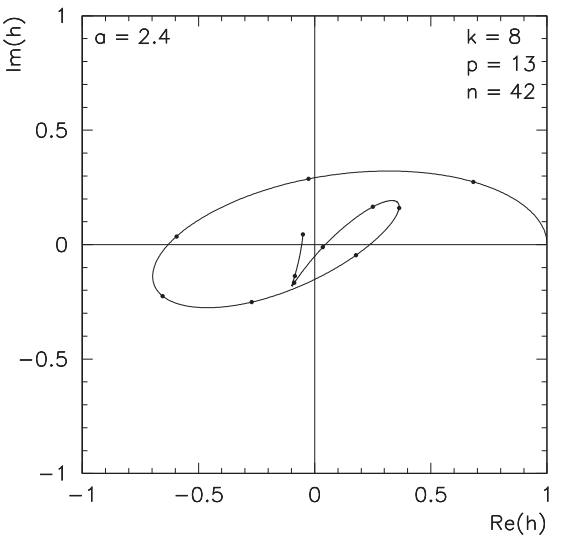

Fig. 16. Parametric curve of the exponential draft function $\tilde{h}(2^{-\hat{p}-1}\pi\hat{a}\omega; t_0)$ for $k = 8$, $p = 13$ and $n = 42$ with reduced coupling $\hat{a} = 2.4$ and $\omega \in [0,1]$. The twelve points represent 12 equidistant values of ω for a fixed value of $\hat{a} = 2.4$.

resummed as an exponential function $\tilde{h}(\omega;t_0) = \exp(i\tilde{h}_z(\omega;t_0))$ where the exponent $\tilde{h}_z(\omega;t_0)$ contains only trees,

$$\begin{aligned}\tilde{h}_z(\omega;t_0) = &-i\omega d + \frac{(-i\omega)^2}{4}\sum d_l^2 + \frac{(-i\omega)^3}{8}\sum d_l^2 d_{l+1}\\ &+\frac{(-i\omega)^4}{16}\sum d_l^2 d_{l+1}d_{l+2} - \frac{(-i\omega)^4}{64}\sum d_l^4\\ &+\frac{(-i\omega)^5}{32}\sum d_l^2 d_{l+1}d_{l+2}d_{l+3}\\ &+\frac{(-i\omega)^5}{384}\sum d_l^4 d_{l+2} - \frac{(-i\omega)^5}{64}\sum d_l^2 d_{l+1}^3\\ &-\frac{(-i\omega)^5}{48}\sum d_l^4 d_{l+1} + \frac{(-i\omega)^6}{64}\sum d_l^2 d_{l+1}d_{l+2}d_{l+3}d_{l+4}\\ &+\frac{(-i\omega)^6}{384}\sum d_l^2 d_{l+1}^3 d_{l+3} + \frac{(-i\omega)^6}{768}\sum d_l^4 d_{l+2}d_{l+3}\\ &-\frac{(-i\omega)^6}{48}\sum d_l^2 d_{l+1}^3 d_{l+2} - \frac{(-i\omega)^6}{96}\sum d_l^4 d_{l+1}d_{l+2}\\ &-\frac{(-i\omega)^6}{128}\sum d_l^2 d_{l+1}d_{l+2}^3 - 11\frac{(-i\omega)^6}{1536}\sum d_l^4 d_{l+1}^2\\ &+\frac{(-i\omega)^6}{576}\sum d_l^6 + \cdots \end{aligned} \tag{33}$$

6.2. Single trees and multiple trees

The idea of using binary forest graphs for our calculation can be summarized as follows: Let d_l be the coefficient of the Chebyshev polynomial $T_{2^l}(\phi_+)$. Under the replacement $\phi_+ = \sin(\pi t_+/2)$ one has $T_{2^0}(\phi_+) = \sin(\pi t_+/2)$, $T_{2^1}(\phi_+) = -\cos(\pi t_+)$, and $T_{2^l}(\phi_+) = \cos(2^{l-1}\pi t_+)$ for $l > 1$. Therefore, under this replacement, the Chebyshev poynomials can be represented using complex exponential functions $\exp(\pm 2^{l-1} i\pi t_+)$. In calculating the integral in Eq. (31), a product of exponential functions corresponding to the coefficients d_{l+i} in the sums in Eq. (32) is integrated over ϕ_+. However, the integration of this product gives a non-vanishing contribution only if the exponent of the complex exponential vanishes (for details, cf. Refs. [30,31]).

To give an example, the l-th contribution to $\sum d_l^2 d_{l+1}$ in Eq. (32) is given by integrals of the exponential function

$$\exp((\pm 2^l \pm 2^l \pm 2^{l+1})i\pi t_+) = \exp(2^l(\pm 2^0 \pm 2^0 \pm 2^1)i\pi t_+). \tag{34}$$

This integral gives a non-vanishing contribution only in the case where $\pm 2^0 \pm 2^0 \pm 2^1 = 0$ (all the signs being independent). The only possibilities in this case are $2^0 + 2^0 - 2^1 = 1 + 1 - 2 = 0$ and $-2^0 - 2^0 + 2^1 = -1 - 1 + 2 = 0$ which are different only by a global sign. One can write $2^0 + 2^0 = 1 + 1 = 2 = 2^1$ which is a unique partition of the highest power. In general, the *binary sum condition* is given by

$$\sum_{m=0}^{i}\sum_{n=1}^{n_m} s_n 2^m = 0 \tag{35}$$

where $s_n = \pm 1$ are the possible signs in the binary sum condition. The same powers of *2* in this condition are represented by points (leaves) in the same layer of a binary forest of graphs. In order to understand these graphs and their construction methods, one starts with the highest power. The highest power 2^i can be decomposed into lower powers by using $2^i = 2^{i-1} + 2^{i-1}$. This is represented by two lines going down from this (highest) point of the graph. If both lower powers are found in the binary sum condition (like in $2^1 = 2^0 + 2^0$ in the example above), the lines are closed by points (leaves are drawn) and a tree is created. If one (or both) of the lower powers are not found in the vanishing sum, this lower power again is decomposed in smaller powers, until the powers are met by contributions in the binary sum condition.

The main part of the exponent $\tilde{h}_z(\omega;t_0)$ contains single trees, corresponding to unique decompositions of the highest power of 2. They are given by

$n = 2$: $\sum d_l^2$ means $1 - 1 = 0$

$n = 3$: $\sum d_l^2 d_{l+1}$ means $1 + 1 - 2 = 0$

$n = 4$: $\sum d_l^2 d_{l+1}d_{l+2}$ means $1 + 1 + 2 - 4 = 0$

$n = 5$: $\sum d_l^2 d_{l+1}d_{l+2}d_{l+3}$ means $1 + 1 + 2 + 4 - 8 = 0$

$\sum d_l^4 d_{l+2}$ means $1 + 1 + 1 + 1 - 4 = 0$

$n = 6$: $\sum d_l^2 d_{l+1}d_{l+2}d_{l+3}d_{l+4}$ means $1 + 1 + 2 + 4 + 8 - 16 = 0$

$\sum d_l^4 d_{l+2}d_{l+3}$ means $1 + 1 + 1 + 1 + 4 - 8 = 0$

$\sum d_l^2 d_{l+1}^3 d_{l+3}$ means $1 + 1 + 2 + 2 + 2 - 8 = 0$

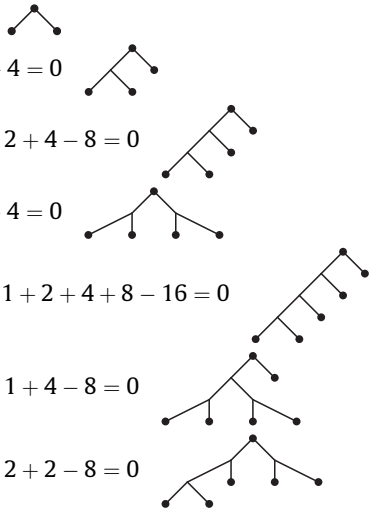

(36)

The coefficients for these contributions are given by

$$\frac{1}{2^{n-1}n_0!n_1!\cdots n_{n-2}!} \tag{37}$$

where n_k counts the occurence of 2^k in the decomposition. However, there are also multiple trees, like for instance $\sum d_l^2 d_{l+1}^3$, corresponding to $+1+1-2|+2-2=0$ where the vertical bar separates the two different independent relations $+1+1-2=0$ and $+2-2=0$. In order to deal with these contributions and their coefficients, it is appropriate to work with so-called summation ordering (for more details see Appendix D).

6.3. Summation ordering

If for multiple sums one excludes repeating indices, one ends up with a summation ordered expression, similar to time ordered expressions in quantum field theory. One obtains

$$\begin{aligned}\tilde{h}(\omega;t_0) = e^{-i\omega d}\Bigg(&1+\frac{(-i\omega)^2}{4}\sum d_l^2+\frac{(-i\omega)^3}{8}\sum d_l^2 d_{l+1}\\
&+\frac{(-i\omega)^4}{16}\sum d_l^3 d_{l+1}d_{l+2}+\frac{(-i\omega)^4}{32}\sum d_l^2{\sum}' d_{l'}^2\\
&+\frac{(-i\omega)^4}{64}\sum d_l^4+\frac{(-i\omega)^5}{32}\sum d_l^2 d_{l+1}d_{l+2}d_{l+3}\\
&+\frac{(-i\omega)^5}{32}\sum d_l^2 d_{l+1}{\sum}' d_{l'}^2+\frac{(-i\omega)^5}{384}\sum d_l^4 d_{l+2}\\
&+\frac{(-i\omega)^5}{64}\sum d_l^2 d_{l+1}^3+\frac{(-i\omega)^5}{96}\sum d_l^4 d_{l+1}\\
&+\frac{(-i\omega)^6}{64}\sum d_l^2 d_{l+1}d_{l+2}d_{l+3}d_{l+4}\\
&+\frac{(-i\omega)^6}{384}\sum d_l^2 d_{l+1}^3 d_{l+3}+\frac{(-i\omega)^6}{768}\sum d_l^4 d_{l+2}d_{l+3}\\
&+\frac{(-i\omega)^6}{96}\sum d_l^2 d_{l+1}^3 d_{l+2}+\frac{(-i\omega)^6}{192}\sum d_l^4 d_{l+1}d_{l+2}\\
&+\frac{(-i\omega)^6}{128}\sum d_l^2 d_{l+1}d_{l+2}^3+\frac{(-i\omega)^6}{1536}\sum d_l^4 d_{l+1}^2\\
&+\frac{(-i\omega)^6}{64}\sum d_l^2 d_{l+1}d_{l+2}{\sum}' d_{l'}^2\\
&+\frac{(-i\omega)^6}{128}\sum d_l^2 d_{l+1}{\sum}' d_{l'}^2 d_{l'+1}+\frac{(-i\omega)^6}{2304}\sum d_l^6\\
&+\frac{(-i\omega)^6}{256}\sum d_l^4{\sum}' d_{l'}^2+\frac{(-i\omega)^6}{384}\sum d_l^2{\sum}' d_{l'}^2{\sum}'' d_{l''}^2+\cdots\Bigg)\end{aligned} \tag{38}$$

$$\begin{aligned}=\mathcal{S}\exp\Bigg(&-i\omega d+\frac{(-i\omega)^2}{4}\sum d_l^2+\frac{(-i\omega)^3}{8}\sum d_l^2 d_{l+1}\\
&+\frac{(-i\omega)^4}{16}\sum d_l^3 d_{l+1}d_{l+2}+\frac{(-i\omega)^4}{64}\sum d_l^4\\
&+\frac{(-i\omega)^5}{32}\sum d_l^2 d_{l+1}d_{l+2}d_{l+3}+\frac{(-i\omega)^5}{384}\sum d_l^4 d_{l+2}\\
&+\frac{(-i\omega)^5}{64}\sum d_l^2 d_{l+1}^3+\frac{(-i\omega)^5}{96}\sum d_l^4 d_{l+1}\\
&+\frac{(-i\omega)^6}{64}\sum d_l^2 d_{l+1}d_{l+2}d_{l+3}d_{l+4}\\
&+\frac{(-i\omega)^6}{384}\sum d_l^2 d_{l+1}^3 d_{l+3}+\frac{(-i\omega)^6}{768}\sum d_l^4 d_{l+2}d_{l+3}\\
&+\frac{(-i\omega)^6}{96}\sum d_l^2 d_{l+1}^3 d_{l+2}+\frac{(-i\omega)^6}{192}\sum d_l^4 d_{l+1}d_{l+2}\\
&+\frac{(-i\omega)^6}{128}\sum d_l^2 d_{l+1}d_{l+2}^3+\frac{(-i\omega)^6}{1536}\sum d_l^4 d_{l+1}^2\\
&+\frac{(-i\omega)^6}{2304}\sum d_l^6+\cdots\Bigg).\end{aligned} \tag{39}$$

Here a prime at the summation symbol means disjunct indices, the symbol $\mathcal{S}$ indicates the summation ordering. Summation ordering defined here, therefore, means that in a product of sums the indices are disjunct. As the time ordering cannot be used directly for the exponent of a time ordered product in quantum field theory, the same holds for the summation ordering: it is defined only if the exponential series in Eq. (39) is expanded as in Eq. (38). However, the coefficients are all positive, and by combinatorical means (worked out in Appendix D), the coefficients of the non-ordered series can be retained.

7. Conclusion

In this paper we have presented novel analytic results for an important class of coupled map lattices (CMLs), so-called chaotic strings, which play an important role in extensions of stochastically quantized field theories. We were able to derive an analytic expression for the invariant 1-point density of the coupled map lattice as a function of the coupling, extending previous results obtained in Refs. [19,20]. The invariant density was approximated to pth order in an iterative recurrence scheme, giving exact result for $p \to \infty$.

This scheme allowed us to better understand the non-trivial dependence of expectations of observables (such as the vacuum expectation value) on the coupling constant. A complex selfsimilar structure was found, for which we developed a mathematical description in terms of scaling functions. Two types of scaling functions were introduced (draft functions and blunt functions) which allowed us to comprehensively describe topological changes, as well as gradual changes, of the generating partition as a function of the coupling a, thus understanding the corresponding changes of the integrals that occur when expectation values are calculated.

Analytical expressions were found for both draft and the blunt functions. Based on these, in the vicinity of local maxima the scale and parameter invariance could be described in an analytic way by introducing a renormalization group 'model' function (the analogue of Feigenbaum's fixed point function for 1-dimensional critical maps). By implementing a graph theoretical method, explicit calculations could be performed for this model function, with surprising connections to Feynman graphs in quantum field theory and other graphs (binary forests) developed to understand the higher-order correlations of uncoupled Chebychev maps. The exponential draft function as the main element of the model function was expressed as a (summation ordered) exponential series.

Our results significantly advance the analytic understanding of chaotic non-hyperbolic CMLs, of relevance in many different areas of physics, and are in good agreement with direct numerical simulations of the CML.

Acknowledgements

This work is supported in part by the Estonian target financed project No. 0180056s09 and by the Estonian Science Foundation under Grant No. 8769. S. Groote

acknowledges support from a grant given by the Deutsche Forschungsgemeinschaft for staying at Mainz University as guest scientist for a couple of months. C. Beck's research is supported by EPSRC.

Appendix A. Explicit calculation for the first and second iterate

In order to explain our method to obtain the first iterate in Eq. (10), we calculate

$$\frac{d}{d\phi}T^{+}_{2a}\big(T^{+}_{2a}(\phi;T_2(\phi_+)+T_2(\phi_-));\phi_++\phi_-\big)= = T^{+\prime}_{2a}(\phi;T_2(\phi_+)+T_2(\phi_-))T^{+\prime}_{2a}\big(T^{+}_{2a}(\phi;T_2(\phi_+) +T_2(\phi_-));\phi_++\phi_-\big). \tag{A1}$$

Close to $\phi = 1$ we obtain

$$T^{+\prime}_{2a}(1-ax;T_2(\phi_+)+T_2(\phi_-))=\frac{1}{4}+O(a),$$
$$T^{+}_{2a}(1-ax;T_2(\phi_+)+T_2(\phi_-))=1-ax'+O(a^2), \tag{A2}$$

where

$$x'=\frac{x}{4}+\frac{1}{8}(T_2(\phi_+)+T_2(\phi_-)-2). \tag{A3}$$

Inserting the positive square root $T^{+}_{2a}(1-ax;T_2(\phi_+)+T_2(\phi_-))\approx 1-ax'$ for ϕ' into the expression $T^{+\prime}_{2a}(\phi';\phi_++\phi_-)$ does not lead to the approximation (2). However, if we insert the negative square root $T^{-}_{2a}(1-ax;T_2(\phi_+)+T_2(\phi_-))\approx -1+ax'$, we obtain

$$T^{+\prime}_{2a}(-1+ax';\phi_++\phi_-)\approx\frac{1}{2\sqrt{2a(1-a)}\sqrt{x/4-r_2^1(\phi_+)-r_2^1(\phi_-)}} \tag{A4}$$

and together with $T^{-\prime}_{2a}(1-ax;T_2(\phi_+)+T_2(\phi_-))\approx -1/4$ the integrand of the first iterate, which is now given by

$$-\frac{d}{d\phi}T^{+}_{2a}\big(T^{-}_{2a}(\phi;T_2(\phi_+)+T_2(\phi_-));\phi_++\phi_-\big). \tag{A5}$$

For the second iterate, we use

$$T^{+\prime}_{2a}(1-ax;T_2(T_2(\phi_+))+T_2(T_2(\phi_-)))=\frac{1}{4}+O(a),$$
$$T^{+}_{2a}(1-ax;T_2(T_2(\phi_+))+T_2(T_2(\phi_-)))=1-ax'+O(a^2),$$
$$T^{-\prime}_{2a}(1-ax';T_2(\phi_+)+T_2(\phi_-))=-\frac{1}{4}+O(a),$$
$$T^{-}_{2a}(1-ax';T_2(\phi_+)+T_2(\phi_-))=-1+ax''+O(a^2) \tag{A6}$$

with

$$x'=\frac{x}{4}+\frac{1}{8}(T_2(T_2(\phi_+))+T_2(T_2(\phi_-))-2),$$
$$x''=\frac{x'}{4}+\frac{1}{8}(T_2(\phi_+)+T_2(\phi_-)-2) \tag{A7}$$

and, finally,

$$T^{-1\prime}_{2a}(-1+ax'';\phi_++\phi_-)\approx\frac{1}{2\sqrt{2a(1-a)}\sqrt{x/16-r_2^2(\phi_+)-r_2^2(\phi_-)}}. \tag{A8}$$

The integrand, therefore, is given by

$$-\frac{d}{d\phi}T^{+}_{2a}\big(T^{+}_{2a}\big(T^{-}_{2a}(\phi;T_2(T_2(\phi_+))+T_2(T_2(\phi_-)));\times T_2(\phi_+)+T_2(\phi_-)\big);\phi_++\phi_-\big). \tag{A9}$$

Appendix B. Details on the "path of the roots"

In Appendix A we have considered only one "path of the roots" which directly leads to the iterates $\rho_a^{(p)}(\phi)$. However, it can be shown that by adding over all possible paths, we end up with Eq. (12) which is equal to $\rho_a^{(0)}(\phi)$ close to the boundary $\phi = -1$ and equal to the sum of the $\rho_a^{(q)}(\phi)$ (for $q\leqslant p$) at the boundary $\phi = +1$. Looking at the region close to the boundary $\phi = -1$, we expand the integrand of (12) with $\phi = ay-1$ for small values of a. Looking at different orders p, we obtain

$$\frac{d}{d\phi}T^{-1}_{2a}(\phi;\phi_++\phi_-):$$
$$=\frac{d}{d\phi}T^{+}_{2a}(\phi;\phi_++\phi_-)+\frac{d}{d\phi}T^{-}_{2a}(\phi;\phi_++\phi_-)$$
$$\approx\frac{1}{\sqrt{16a(1-a)(y-r_2^0(\phi_+)-r_2^0(\phi_-))}}$$
$$=\frac{1}{\sqrt{8a(1-a)(y-r_2^0(\phi_+)-r_2^0(\phi_-))}}\sin\left(\frac{\pi}{4}\right),$$

$$\frac{d}{d\phi}T^{-1}_{2a}(T^{-1}_{2a}(\phi;T_2(\phi_+)+T_2(\phi_-));\phi_++\phi_-):$$
$$=\frac{d}{d\phi}T^{+}_{2a}(T^{+}_{2a}(\phi;T_2(\phi_+)+T_2(\phi_-));\phi_++\phi_-)$$
$$+\frac{d}{d\phi}T^{+}_{2a}(T^{-}_{2a}(\phi;T_2(\phi_+)+T_2(\phi_-));\phi_++\phi_-)$$
$$+\frac{d}{d\phi}T^{-}_{2a}(T^{+}_{2a}(\phi;T_2(\phi_+)+T_2(\phi_-));\phi_++\phi_-)$$
$$+\frac{d}{d\phi}T^{-}_{2a}(T^{-}_{2a}(\phi;T_2(\phi_+)+T_2(\phi_-));\phi_++\phi_-)$$
$$\approx\frac{1}{\sqrt{8a(1-a)(y-r_2^0(\phi_+)-r_2^0(\phi_-))}}\times\frac{1}{2}\left(\frac{1}{\sqrt{2}\sqrt{2+\sqrt{2}}}+\frac{1}{\sqrt{2}\sqrt{2-\sqrt{2}}}\right)$$
$$=\frac{1}{\sqrt{8a(1-a)(y-r_2^0(\phi_+)-r_2^0(\phi_-))}}\times\frac{1}{2}\left(\sin\left(\frac{\pi}{8}\right)+\sin\left(\frac{3\pi}{8}\right)\right),$$

$$
\begin{aligned}
&\frac{d}{d\phi}T_{2a}^{-1}\Big(T_{2a}^{-1}\Big(T_{2a}^{-1}(\phi;T_2(T_2(\phi_+))+T_2(T_2(\phi_-)));\\
&T_2(\phi_+)+T_2(\phi_-)\Big);\phi_++\phi_-\Big)\\
&:=\frac{d}{d\phi}T_{2a}^{+}\Big(T_{2a}^{+}\Big(T_{2a}^{+}(\phi;T_2(T_2(\phi_+))+T_2(T_2(\phi_-)));\\
&T_2(\phi_+)+T_2(\phi_-)\Big);\phi_++\phi_-\Big)\\
&+\frac{d}{d\phi}T_{2a}^{+}\Big(T_{2a}^{+}\Big(T_{2a}^{-}(\phi;T_2(T_2(\phi_+))+T_2(T_2(\phi_-)));T_2(\phi_+)\\
&+T_2(\phi_-));\phi_++\phi_-\Big)+\frac{d}{d\phi}T_{2a}^{+}\Big(T_{2a}^{-}\Big(T_{2a}^{+}(\phi;T_2(T_2(\phi_+))\\
&+T_2(T_2(\phi_-)));T_2(\phi_+)+T_2(\phi_-)\Big);\phi_++\phi_-\Big)\\
&+\frac{d}{d\phi}T_{2a}^{+}\Big(T_{2a}^{-}\Big(T_{2a}^{-}(\phi;T_2(T_2(\phi_+))+T_2(T_2(\phi_-)));T_2(\phi_+)\\
&+T_2(\phi_-));\phi_++\phi_-\Big)+\frac{d}{d\phi}T_{2a}^{-}\Big(T_{2a}^{+}\Big(T_{2a}^{+}(\phi;T_2(T_2(\phi_+))\\
&+T_2(T_2(\phi_-)));T_2(\phi_+)+T_2(\phi_-)\Big);\phi_++\phi_-\Big)\\
&+\frac{d}{d\phi}T_{2a}^{-}\Big(T_{2a}^{+}\Big(T_{2a}^{-}(\phi;T_2(T_2(\phi_+))+T_2(T_2(\phi_-)));T_2(\phi_+)\\
&+T_2(\phi_-));\phi_++\phi_-\Big)+\frac{d}{d\phi}T_{2a}^{-}\Big(T_{2a}^{-}\Big(T_{2a}^{+}(\phi;T_2(T_2(\phi_+))\\
&+T_2(T_2(\phi_-)));T_2(\phi_+)+T_2(\phi_-)\Big);\phi_++\phi_-\Big)\\
&+\frac{d}{d\phi}T_{2a}^{-}\Big(T_{2a}^{-}\Big(T_{2a}^{-}(\phi;T_2(T_2(\phi_+))+T_2(T_2(\phi_-)));T_2(\phi_+)\\
&+T_2(\phi_-));\phi_++\phi_-\Big)\approx\frac{1}{\sqrt{8a(1-a)(y-r_2^0(\phi_+)-r_2^0(\phi_-))}}\\
&\times\frac{1}{4}\left(\frac{1}{\sqrt{2}\sqrt{2+\sqrt{2}}\sqrt{2+\sqrt{2+\sqrt{2}}}}\right.\\
&+\frac{1}{\sqrt{2}\sqrt{2-\sqrt{2}}\sqrt{2+\sqrt{2-\sqrt{2}}}}\\
&+\frac{1}{\sqrt{2}\sqrt{2+\sqrt{2}}\sqrt{2-\sqrt{2+\sqrt{2}}}}\\
&\left.+\frac{1}{\sqrt{2}\sqrt{2-\sqrt{2}}\sqrt{2-\sqrt{2-\sqrt{2}}}}\right)\\
&=\frac{1}{\sqrt{8a(1-a)(y-r_2^0(\phi_+)-r_2^0(\phi_-))}}\\
&\times\frac{1}{4}\left(\sin\left(\frac{\pi}{16}\right)+\sin\left(\frac{3\pi}{16}\right)+\sin\left(\frac{7\pi}{16}\right)+\sin\left(\frac{5\pi}{16}\right)\right). \qquad \text{(B1)}
\end{aligned}
$$

For obtaining the final results we have used that

$$
\begin{aligned}
&\frac{1}{\sqrt{2}}=\sin\left(\frac{\pi}{4}\right),\\
&\frac{1}{\sqrt{2}\sqrt{2+\sqrt{2}}}=\frac{1}{2}\sqrt{2-\sqrt{2}}=\sin\left(\frac{\pi}{8}\right),\\
&\frac{1}{\sqrt{2}\sqrt{2-\sqrt{2}}}=\frac{1}{2}\sqrt{2+\sqrt{2}}=\sin\left(\frac{3\pi}{8}\right),\\
&\frac{1}{\sqrt{2}\sqrt{2+\sqrt{2}}\sqrt{2+\sqrt{2+\sqrt{2}}}}\\
&=\frac{1}{2}\sqrt{2}\sqrt{2+\sqrt{2}}\sqrt{2-\sqrt{2+\sqrt{2}}}=\sin\left(\frac{\pi}{16}\right),\\
&\frac{1}{\sqrt{2}\sqrt{2-\sqrt{2}}\sqrt{2+\sqrt{2-\sqrt{2}}}}\\
&=\frac{1}{2}\sqrt{2}\sqrt{2-\sqrt{2}}\sqrt{2-\sqrt{2-\sqrt{2}}}=\sin\left(\frac{3\pi}{16}\right),\\
&\frac{1}{\sqrt{2}\sqrt{2+\sqrt{2}}\sqrt{2-\sqrt{2+\sqrt{2}}}}\\
&=\frac{1}{2}\sqrt{2}\sqrt{2+\sqrt{2}}\sqrt{2+\sqrt{2+\sqrt{2}}}=\sin\left(\frac{7\pi}{16}\right),\\
&\frac{1}{\sqrt{2}\sqrt{2-\sqrt{2}}\sqrt{2-\sqrt{2-\sqrt{2}}}}\\
&=\frac{1}{2}\sqrt{2}\sqrt{2-\sqrt{2}}\sqrt{2+\sqrt{2-\sqrt{2}}}=\sin\left(\frac{5\pi}{16}\right). \qquad \text{(B2)}
\end{aligned}
$$

Because of

$$
\frac{1}{2^p}\sum_{m=0}^{2^p-1}\sin\left(\frac{\pi(2m+1)}{2^{p+2}}\right)\to\int_0^1\sin\left(\frac{\pi t}{2}\right)dt=\frac{2}{\pi}, \qquad \text{(B3)}
$$

for higher and higher orders of p the integrand approaches

$$
\begin{aligned}
&\frac{2}{\pi}\frac{1}{\sqrt{8a(1-a)(y-r_2^0(\phi_+)-r_2^0(\phi_-))}}\\
&=\frac{1}{\pi\sqrt{2a(1-a)(y-r_2^0(\phi_+)-r_2^0(\phi_-))}}. \qquad \text{(B4)}
\end{aligned}
$$

Similar considerations lead to the iterates close to the boundary $\phi = +1$.

Appendix C. The model function for $p \to \infty$

Because the second part of the radicand in Eq. (22) contains a k-fold Chebychev map, one first has to unfold this map. Using

$$
\phi_\pm=\sin\left(\frac{\pi}{2}t_\pm\right), \qquad \rho_0(\phi_\pm)d\phi_\pm=\frac{1}{2}dt_\pm, \qquad \text{(C1)}
$$

one obtains

$$
\hat{f}^{(\hat{p},k)}(\Delta\hat{t};t_0)=\frac{1}{4}\int_{-1}^{1}dt_+dt_-\times\cos\left(\sqrt{\pi^2\left(\Delta\hat{t}-2^{-\hat{p}}\hat{a}\tilde{\tilde{d}}^{(k)}(t_0;t_+,t_-)\right)^2-2\hat{a}r_2^{\infty}\left(-\cos(2^{k-1}\pi t_+),-\cos(2^{k-1}\pi t_-)\right)}\right). \qquad \text{(C2)}
$$

After the substitution $t'_\pm=2^k t_\pm$ the result reads

$$\hat{f}^{(\hat{p},k)}(\Delta\hat{t};t_0)=\frac{1}{4^{k+1}}\int_{-2^k}^{2^k}dt'_+dt'_-\times\cos\left(\sqrt{\pi^2\left(\Delta\hat{t}-2^{-\hat{p}}\hat{a}\tilde{\hat{d}}^{(k)}\left(t_0;2^{-k}t'_+,2^{-k}t'_-\right)\right)^2-2\hat{a}r_2^{\infty}\left(-\cos(\frac{\pi}{2}t'_+),-\cos\left(\frac{\pi}{2}t'_-\right)\right)}\right). \tag{C3}$$

The huge integration range $[-2^k,2^k]$ for each of $\phi'_\pm$ can be divided up into the standard intervals $[-1,+1]$ by using

$$t''_\pm=t'_\pm+2^k-2n_\pm-1\in[-1,+1], \tag{C4}$$

where $n_\pm=0,1,\ldots,2^k-1$ counts the intervals. Because of $t_\pm=2^{-k}(t''_\pm+2n_\pm+1)-1$, the (twofold linearized) draft function $\tilde{\hat{d}}^{(k)}(t_0;t_+,t_-)$ is nearly constant in each of the intervals $[-1,+1]$. In defining

$$\hat{d}_{n_+n_-}(t_0):=\lim_{k\to\infty}\tilde{\hat{d}}^{(k)}(t_0;2^{-k}(2n_++1)-1,2^{-k}(2n_-+1)-1) \tag{C5}$$

one has to deal only with the blunt. Using

$$\begin{aligned}-\cos\left(\frac{\pi}{2}t'_\pm\right)&=-\cos\left(\frac{\pi}{2}t''_\pm-\frac{\pi}{2}(2^k-1-2n_\pm)\right)\\&=-\cos\left(\frac{\pi}{2}t'_\pm-2^{k-1}\pi+\frac{\pi}{2}+\pi n_\pm\right)\\&=\sin\left(\frac{\pi}{2}t''_\pm+\pi n_\pm\right)=(-1)^{n_\pm}\sin\left(\frac{\pi}{2}t''_\pm\right)\end{aligned} \tag{C6}$$

and removing the sign by replacing $t''_\pm\to-t''_\pm$, for the limit $k\to\infty$ one obtains

$$\begin{aligned}\hat{f}^{(\hat{p})}(\Delta\hat{t};t_0)&=\lim_{k\to\infty}\frac{1}{4^{k+1}}\sum_{n_\pm=0}^{2^k-1}\int_{-1}^{1}dt''_+dt''_-\times\cos\left(\sqrt{\pi^2\left(\Delta\hat{t}-2^{-\hat{p}}\hat{a}\hat{d}_{n_+n_-}(t_0)\right)^2-2\hat{a}r_2^{\infty}\left(\sin\left(\frac{\pi}{2}t''_+\right),\sin\left(\frac{\pi}{2}t''_-\right)\right)}\right)\\&=\lim_{k\to\infty}\frac{1}{4^k}\sum_{n_\pm=0}^{2^k-1}\int\rho_0(\phi_+)d\phi_+\rho_0(\phi_-)d\phi_-\times\cos\left(\sqrt{\pi^2\left(\Delta\hat{t}-2^{-\hat{p}}\hat{a}\hat{d}_{n_+n_-}(t_0)\right)^2-2\hat{a}r_2^{\infty}(\phi_+,\phi_-)}\right).\end{aligned} \tag{C7}$$

In the final step, $\phi_\pm=\sin(\pi t''_\pm/2)$ is used. The integrand does depend on $\phi_\pm$ only via $r_2^{\infty}(\phi_+,\phi_-)$ while for the first part one can use the abbreviation

$$\hat{c}=\pi\left(\Delta\hat{t}-2^{-\hat{p}}\hat{a}\hat{d}_{n_+n_-}(t_0)\right). \tag{C8}$$

In Fig. 17 the function

$$g^{(p)}(\hat{a},\hat{c}):=\int\rho_0(\phi_+)d\phi_+\rho_0(\phi_-)d\phi_-\cos\left(\sqrt{\hat{c}^2-2\hat{a}r_2^{p}(\phi_+,\phi_-)}\right) \tag{C9}$$

is shown as a function of $\hat{c}$ for different values of $\hat{a}$. For the order p of the blunt function $r_2^p(\phi_+,\phi_-)$ a value of $p=3$ is enough to provide sufficient precision. In analysing the position of the drafted minima in dependence on $\hat{a}$, one obtains[4]

$$\hat{c}(\hat{a})^2-\hat{c}(0)^2=-\frac{8\hat{a}}{3}\Longleftrightarrow\hat{c}(0)=\sqrt{\hat{c}(\hat{a})^2+\frac{8\hat{a}}{3}}, \tag{C10}$$

leading to

$$g^{(p)}(\hat{a},\hat{c})=\cos\left(\sqrt{\hat{c}^2+\frac{8\hat{a}}{3}}\right). \tag{C11}$$

This function can be inserted into Eq. (C7) to give

$$\hat{f}^{(\hat{p})}(\Delta\hat{t};t_0)=\lim_{k\to\infty}\frac{1}{4^k}\sum_{n_\pm=0}^{2^k-1}\cos\left(\sqrt{\pi^2\left(\Delta\hat{t}-2^{-\hat{p}}\hat{a}\hat{d}_{n_+n_-}(t_0)\right)+\frac{8\hat{a}}{3}}\right). \tag{C12}$$

In the limit $k\to\infty$, the remaining summations over $n_\pm$ can be reunited to an integration over $\phi_\pm$, leading to the final result in Eq. (23). For practical reasons, however, k is kept finite in the main text.

Appendix D. Combinatorics for the exponential draft function

The (positive) coefficients of the exponent of the summation ordered exponential draft function can be calculated by using combinatorial considerations. In this appendix we demonstrate the procedure for single and multiple trees in the summation ordered expression and show how to derive the coefficients of the non-ordered expression.

D.1. Coefficients for single trees

According to our graph theory, single binary trees represent unique relations between powers of 2. The sum

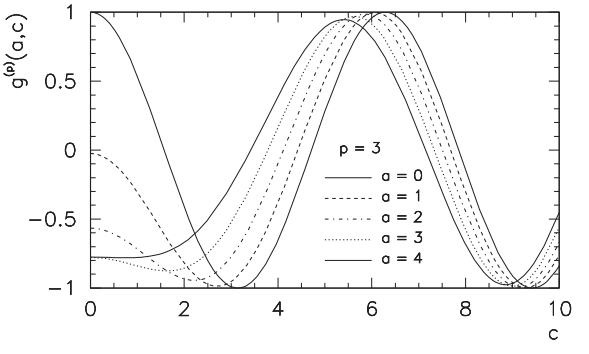

Fig. 17. $g^{(p)}(\hat{a},\hat{c})$ as a function of $\hat{c}$ for different values of $\hat{a}$. The order p of the blunt function $r_2^p(\phi_+,\phi_-)$ is chosen to be $p=3$.

[4] The value $-8/3$ is not rigorously derived but follows from numerical inspection.

$\sum d_l^2 d_{l+1}^3 d_{l+3}$ for instance, represented by the single tree

results from the unique relation $1+1+2+2+2-8=0$. In general, from combinatorics one can see that for the expression

$$\sum_{l=0}^{k-n+1}\prod_{i=0}^{n-2} d_{l+i}^{n_i}, \qquad \sum_{i=0}^{n-2} n_i = n \tag{D1}$$

there are $n!/(n_0!n_1!\cdots n_{n-2}!)$ discriminable permutations without taking into account the global sign (which gives a factor 2!). Together with a factor $1/n!$ for the exponential series in Eq. (31 and a factor $1/2^n$ from the trigonometric functions $T_{2^l}(\sin(\pi t_+/2))$ after their expansion in exponential functions, one obtains

$$\frac{1}{n!2^n}\left(\frac{2!n!}{n_0!n_1!\cdots n_{n-2}!}\right) = \frac{1}{2^{n-1}n_0!n_1!\cdots n_{n-2}!}. \tag{D2}$$

D.2. Coefficients for multiple trees

While the coefficients of the single tree contributions are the same for the summation ordered as for the non-ordered exponential draft function, the coefficients of the multiple tree contributions are different in both cases. However, the coefficients of the summation ordered contributions can be calculated by combinatorial means. This is shown for the contributions of orders $n=4$ to 6 in the following. Multiple binary trees correspond to relations between powers of 2 which can be split into two or more single relations separated by a vertical bar.

- $\sum d_l^4$: $+1-1|+1-1=0$ gives 4!/2!/2! permutation if +1 and −1 are taken to be two different elements. A global sign for the first or the second part $+1-1=0$ need not be taken into account because the permutations already lead to the sign-changed contributions (sign non-sensitive). Together with the global factor $1/4!/2^4$ one obtains

$$\frac{1}{4!2^4}\left(\frac{4!}{2!2!}\right) = \frac{1}{2^4 2!2!} = \frac{1}{64}.$$

- $\sum d_l^4 d_{l+1}$: $+1+1-2|+1-1=0$ gives 5!/3!1!1! permutations where now the global sign for the first part has to be taken into account. One obtains two (formally equal) contributions

$$\frac{1}{5!2^5}\left(\frac{5!}{3!1!1!}+\frac{5!}{1!3!1!}\right) = \frac{2}{2^5 3!} = \frac{1}{96}.$$

- $\sum d_l^2 d_{l+1}^3$: $+1+1-2|+2-2=0$ gives 5!/2!1!2! permutations where the same holds as in the previous case. One obtains

$$\frac{1}{5!2^5}\left(\frac{5!}{2!1!2!}+\frac{5!}{2!2!1!}\right) = \frac{2}{2^5 2!2!} = \frac{1}{128}.$$

- $\sum d_l^2 d_{l+1}^3 d_{l+2}$: $+1+1-2|+2+2-4=0$ gives 6!/2!1!2!1! permutations. In this case one has to take into account the global signs of both parts. In addition the numer of elements changes if the global signs change. One obtains

$$\frac{1}{6!2^6}\left(\frac{6!}{2!1!2!1!}+\frac{6!}{2!3!1!}+\frac{6!}{2!1!2!1!}+\frac{6!}{2!3!1!}\right) = \frac{1}{96}.$$

- $\sum d_l^4 d_{l+1} d_{l+2}$: $+1-1|+1+1+2-4=0$ gives

$$\frac{1}{6!2^6}\left(\frac{6!}{3!1!1!1!}+\frac{6!}{1!3!1!1!}\right) = \frac{1}{192}.$$

- $\sum d_l^2 d_{l+1} d_{l+2}^3$: $+1+1+2-4|+4-4=0$ gives

$$\frac{1}{6!2^6}\left(\frac{6!}{2!1!1!2!}+\frac{6!}{2!1!2!1!}\right) = \frac{1}{128}.$$

- $\sum d_l^4 d_{l+1}^2$: Besides the sign sensitive possibility $+1+1-2|+1+1-2=0$, in principle there is also a non-sensitive possibility with three parts, $+1-1|+1-1|+2-1=0$. However, this possibility is the same as the sign-changed possibility $+1+1-2|-1-1+2=0$. Therefore, only the first has to be taken into account, resulting in

$$\frac{1}{6!2^6}\left(\frac{6!}{4!2!}+\frac{6!}{2!2!1!1!}+\frac{6!}{2!2!1!1!}+\frac{6!}{4!2!}\right) = \frac{1}{1536}.$$

- $\sum d_l^6$: $+1-1|+1-1|+1-1=0$ contains three parts not sensitive to the global signs. Therefore, one obtains

$$\frac{1}{6!2^6}\left(\frac{6!}{3!3!}\right) = \frac{1}{2304}.$$

D.3. Summation ordered and non-ordered coefficients

The relation between the coefficients of the summation ordered and non-ordered exponential draft function can be found by using

$$\begin{aligned}
&\sum d_l^2 \sum d_{l'}^2 = \sum d_l^2 \sum{}' d_{l'}^2 + \sum d_l^4,\\
&\sum d_l^2 d_{l+1} \sum d_{l'}^2 = \sum d_l^2 d_{l+1} \sum{}' d_{l'}^2 + \sum d_l^4 d_{l+1} + \sum d_l^2 d_{l+1}^3,\\
&\sum d_l^2 d_{l+1} d_{l+2} \sum d_{l'}^2 = \sum d_l^2 d_{l+1} d_{l+2} \sum{}' d_{l'}^2 + \sum d_l^4 d_{l+1} d_{l+2},\\
&\qquad + \sum d_l^2 d_{l+1}^3 d_{l+2} + \sum d_l^2 d_{l+1} d_{l+2}^3,\\
&\sum d_l^2 d_{l+1} \sum d_{l'}^2 d_{l'+1}\\
&\quad = \sum d_l^2 d_{l+1} \sum{}' d_{l'}^2 d_{l'+1} + \sum d_l^2 d_{l+1}^3 d_{l+2} + \sum d_l^4 d_{l+1}^2 + \sum d_{l'}^2 d_{l'+1}^3 d_{l'+2}\\
&\quad = \sum d_l^2 d_{l+1} \sum{}' d_{l'}^2 d_{l'+1} + \sum d_l^4 d_{l+1}^2 + 2\sum d_l^2 d_{l+1}^3 d_{l+2},\\
&\sum d_l^4 \sum d_{l'}^2 = \sum d_l^4 \sum{}' d_{l'}^2 + \sum d_l^6,\\
&\sum d_l^2 \sum d_{l'}^2 \sum d_{l''}^2 = \left(\sum d_l^2 \sum{}' d_{l'}^2\right) \sum d_{l''}^2 + \sum d_l^4 \sum d_{l'}^2\\
&\quad = \sum d_l^2 \sum{}' d_{l'}^2 \sum{}'' d_{l''}^2 + \sum d_l^2 \sum{}' d_{l'}^4 + \sum d_l^4 \sum{}' d_{l'}^2 + \sum d_{l'}^4 \sum{}' d_{l''}^2 + \sum d_l^6 =\\
&\quad = \sum d_l^2 \sum{}' d_{l'}^2 \sum{}'' d_{l''}^2 + 3\sum d_l^4 \sum{}' d_{l'}^2 + \sum d_l^6.
\end{aligned} \tag{D3}$$

Using, for instance, for the contribution of order $n=6$ in Eq. (32) a general ansatz and applying Eqs. (D3), one obtains

$$
\begin{aligned}
&A_1 \sum d_l^2 d_{l+1} d_{l+2} d_{l+3} d_{l+4} + A_2 \sum d_l^2 d_{l+1}^3 d_{l+3} + A_3 \\
&\quad \times \sum d_l^4 d_{l+2} d_{l_3} + A_4 \sum d_l^2 d_{l+1}^3 d_{l+2} + A_5 \\
&\quad \times \sum d_l^4 d_{l+1} d_{l_2} + A_6 \sum d_l^2 d_{l+1} d_{l+2}^2 + A_7 \sum d_l^4 d_{l+1}^2 \\
&\quad + A_8 \sum d_l^2 d_{l+1} d_{l+2} \sum d_{l'}^2 + A_9 \sum d_l^2 d_{l+1} \sum d_{l'}^2 d_{l'+1} \\
&\quad + A_{10} \sum d_l^6 + A_{11} \sum d_l^4 \sum d_{l'}^2 + A_{12} \sum d_l^2 \sum d_{l'}^2 \\
&\quad \times \sum d_{l''}^2 \\
&\quad = A_1 \sum d_l^2 d_{l+1} d_{l+2} d_{l+3} d_{l+4} + A_2 \sum d_l^2 d_{l+1}^3 d_{l+3} + A_3 \\
&\qquad \times \sum d_l^4 d_{l+2} d_{l_3} + (A_4 + A_8 + 2A_9) \sum d_l^2 d_{l+1}^3 d_{l+2} \\
&\qquad + (A_5 + A_8) \sum d_l^4 d_{l+1} d_{l_2} + (A_6 + A_8) \\
&\qquad \times \sum d_l^2 d_{l+1} d_{l+2}^2 + A_7 \sum d_l^4 d_{l+1}^2 + A_8 \\
&\qquad \times \sum d_l^2 d_{l+1} d_{l+2} \sum{}' d_{l'}^2 + A_9 \sum d_l^2 d_{l+1} \sum{}' d_{l'}^2 d_{l'+1} \\
&\qquad + (A_{10} + A_{11} + A_{12}) \sum d_l^6 + (A_{11} + 3A_{12}) \\
&\qquad \times \sum d_l^4 \sum{}' d_{l'}^2 + A_{12} \sum d_l^2 \sum{}' d_{l'}^2 \sum{}'' d_{l''}^2 . \qquad \text{(D4)}
\end{aligned}
$$

Comparing with Eq. (38) one obtains

$$
\begin{aligned}
&A_1 = \frac{1}{64}, \quad A_2 = \frac{1}{384}, \quad A_3 = \frac{1}{768}, \\
&A_8 = \frac{1}{64}, \quad A_9 = \frac{1}{128}, \quad A_{12} = \frac{1}{384}, \qquad \text{(D5)}
\end{aligned}
$$

furthermore

$$
A_{11} = \frac{1}{256} - 3A_{12} = \frac{1}{256} - \frac{1}{128} = -\frac{1}{256},
$$

and finally the coefficients for ...

$$
\begin{aligned}
&\textstyle\sum d_l^2 d_{l+1}^3 d_{l+2}: \quad A_4 = \frac{1}{96} - A_8 - 2A_9 = \frac{1}{96} - \frac{1}{64} - 2\frac{1}{128} = -\frac{1}{48}, \\
&\textstyle\sum d_l^4 d_{l+1} d_{l+2}: \quad A_5 = \frac{1}{192} - A_8 = \frac{1}{192} - \frac{1}{64} = -\frac{1}{96}, \\
&\textstyle\sum d_l^2 d_{l+1} d_{l+2}^3: \quad A_6 = \frac{1}{128} - A_8 = \frac{1}{128} - \frac{1}{64} = -\frac{1}{128}, \\
&\textstyle\sum d_l^4 d_{l+1}^2: \quad A_7 = \frac{1}{1536} - A_9 = \frac{1}{1536} - \frac{1}{128} = -\frac{11}{1536}, \\
&\textstyle\sum d_l^6: \quad A_{10} = \frac{1}{2304} - A_{11} - A_{12} = \frac{1}{2304} + \frac{1}{256} - \frac{1}{384} = \frac{1}{576}. \qquad \text{(D6)}
\end{aligned}
$$

References

[1] Kaneko K. Period-doubling of kink–antikink patterns, quasiperiodicity in antiferro-like structures and spatial intermittency in coupled logistic lattice – towards a prelude of a 'field theory of chaos'. Progr Theoret Phys 1984;72:480–6.
[2] Kapral R. Pattern formation in two-dimensional arrays of coupled, discrete-time oscillators. Phys Rev A 1985;31:3868–79.
[3] Kaneko K, editor. Theory and applications of coupled map lattices. New York: John Wiley and Sons; 1993.
[4] Beck C. Spatio-temporal chaos and vacuum fluctuations of quantized fields. Singapore: World Scientific; 2002.
[5] Bunimovich A, Sinai YaG. Spacetime chaos in coupled map lattices. Nonlinearity 1988;1:491–516.
[6] Amritkar RE, Gade PM. Wavelength doubling bifurcations in coupled map lattices. Phys Rev Lett 1993;70:3408–11.
[7] Carretero-Gonzáles R, Arrowsmith DK, Vivaldi F. Mode-locking in coupled map lattices. Physica D 1997;103:381–403.
[8] Bunimovich LA. Coupled map lattices: Some topological and ergodic properties. Physica D 1997;103:1–17.
[9] Baladi V, Rugh HH. Floquet Spectrum of Weakly Coupled Map Lattices. Commun Math Phys 2001;220:561–82.
[10] Bricmont J, Kupiainen A. High temperature expansions and dynamical systems. Commun Math Phys 1996;178:703–32.
[11] Järvenpää E, Järvenpää M. On the Definition of SRB-Measures for Coupled Map Lattices. Commun Math Phys 2001;220:1–12.
[12] Daido H. Coupling Sensitivity of Chaos – A New Universal Property of Chaotic Dynamical Systems. Progr Theoret Phys Suppl 1984;79:75–95.
[13] Lemaître A, Chaté H. Nonperturbative Renormalization Group for Chaotic Coupled Map Lattices. Phys Rev Lett 1998;80:5528–31.
[14] Lemaître A, Chaté H. Phase Ordering and Onset of Collective Behavior in Chaotic Coupled Map Lattices. Phys Rev Lett 1999;82:1140–3.
[15] Yang W, Ding E-Jiang, Ding M. Universal Scaling Law for the Largest Lyapunov Exponent in Coupled Map Lattices. Phys Rev Lett 1996;76:1808–11.
[16] Torcini A, Livi R, Politi A, Ruffo S. Comment on 'Universal Scaling Law for the Largest Lyapunov Exponent in Coupled Map Lattices. Phys Rev Lett 1997;78. 1391-1391.
[17] Mackey MC, Milton J. Asymptotic stability of densities in coupled map lattices. Physica D 1995;80:1–17.
[18] Beck C. Chaotic strings and standard model parameters. Physica D 2002;171:72–106.
[19] Groote S, Beck C. Scaling behavior of non-hyperbolic coupled map lattices. Phys Rev E 2006;74:046216.
[20] Groote S, Beck C. Scaling properties of invariant densities of coupled Chebyshev maps. Dyn Syst 2007;22:219–48.
[21] Beck C. Statistical mechanics of the vacuum. Mod Phys Lett B 2012;26:1250060.
[22] Parisi G, Wu YS. Perturbation theory without gauge fixing. Sci Sin 1981;24:483.
[23] Damgaard PH, Hüffel H. Stochastic Quantization. Singapore: World Scientific; 1988.
[24] Beck C. Chaotic quantization of field theories. Nonlinearity 1995;8:423–41.
[25] Beck C. Chaotic scalar fields as models for dark energy. Phys Rev D 2004;69:123515.
[26] Dettmann CP. Stable synchronised states of coupled Tchebyscheff maps. Physica D 2002;172:88–102.
[27] Dettmann CP, Lippolis D. Periodic orbit theory of two coupled Tchebyscheff maps. Chaos Soliton Fract 2005;23:43–54.
[28] Maher M, Beck C. Chaotic quantization and the mass spectrum of fermions. Chaos Soliton Fract 2008;37:9–15.
[29] Groote S, Veermäe H. Short chaotic strings and their behaviour in the scaling region. Chaos Soliton Fract 2009;41:2354–9.
[30] Beck C. Higher correlation functions of chaotic dynamical systems – a graph theoretical approach. Nonlinearity 1991;4:1131.
[31] Hilgers A, Beck C. Higher-order correlations of Tchebyscheff maps. Physica D 2001;156:1.
[32] Feigenbaum MJ. Quantitative universality for a class of nonlinear transformations. J Stat Phys 1978;19:25–52.
[33] Feigenbaum MJ. The universal metric properties of nonlinear transformations. J Stat Phys 1979;21:669–706.
[34] Beck C, Schlögl F. Thermodynamics of chaotic systems. Cambridge: Cambridge University Press; 1993.